International Journal of
Molecular Sciences

MDPI

Article

Onconase Induces Apoptosis in Dabrafenib-Resistant Melanoma Cell Lines Through Dysregulation of ROS Homeostasis, Antioxidant Protein Expression, and Mitochondrial Dynamics

Carlotta Passarini †, Alessia Cardile †, Filippo Zuanetti, Valentina Zanrè, Raffaella Pacchiana, Adriana Celesia, Federica Danzi, Alessandra Fiore, Giovanni Gotte * and Marta Menegazzi *

Biological Chemistry Section, Department of Neuroscience, Biomedicine and Movement Science, University of Verona, Strada Le Grazie, 8, I-37134 Verona, Italy; carlotta.passarini@univr.it (C.P.); alessia.cardile@univr.it (A.C.); filippo.zuanetti@univr.it (F.Z.); valentina.zanre@univr.it (V.Z.); raffaella.pacchiana@univr.it (R.P.); adriana.celesia@univr.it (A.C.); federica.danzi@univr.it (F.D.); alessandra.fiore@univr.it (A.F.)

* Correspondence: giovanni.gotte@univr.it (G.G.); marta.menegazzi@univr.it (M.M.)

† These authors contributed equally to this work.

Abstract

Advanced melanoma remains difficult to treat due to its intrinsic resistance to conventional therapies and the frequent development of acquired resistance to targeted agents, such as BRAF inhibitors. Onconase (ONC), an amphibian ribonuclease with established antitumor activity, had been previously shown to have selective cytotoxicity toward melanoma cells. In this study, we investigated the molecular mechanisms underlying ONC-induced cytotoxicity in BRAF-mutated melanoma cell lines that are either sensitive or resistant to the BRAF inhibitor dabrafenib. We focused on oxidative stress regulation, mitochondrial dynamics, and cell death-related signaling pathways. ONC treatment resulted in a marked increase in reactive oxygen species (ROS) levels, concomitant with a pronounced downregulation of NRF2 and multiple NRF2-dependent antioxidant proteins. These effects were particularly evident in dabrafenib-resistant melanoma cells. In parallel, ONC impaired mitochondrial plasticity by inhibiting mitochondrial biogenesis and fission, as evidenced by reduced PGC1α, DRP1, and FIS1 expression. Confocal analysis confirmed the presence of more enlarged mitochondria in ONC-treated cells. Mitophagy and autophagy are hindered by ONC due to the downregulation of PINK1, beclin1, ATG3 expression, as well as the lack of LC3B activation. These mitochondrial defects were associated with mitochondrial-dependent apoptosis, characterized by caspase-9 activation and strong downregulation of the antiapoptotic protein survivin. Lipid peroxidation was also induced by ONC, especially in the A375 cell line. Additionally, ONC inhibited key proliferation-related signaling pathways, including STAT3 and NF-κB, and reduced cyclin-dependent kinase 1, 2, and 4 activities. Collectively, these findings demonstrate that ONC disrupts redox homeostasis, mitochondrial function, and survival signaling in melanoma cells, exerting particularly potent effects in BRAF inhibitor-resistant populations. This study provides mechanistic insight into the anti-melanoma activity of ONC and supports its potential therapeutic application in drug-resistant melanoma.

Keywords: HO-1; GCLM; SOD2; FSP1; SLC7A11; OPA1; DRP1; c-Myc; PINK1; survivin

Academic Editor: Marcus Krüger

Received: 30 December 2025
Revised: 1 February 2026
Accepted: 5 February 2026
Published: 7 February 2026

1. Introduction

Melanoma represents the most aggressive and lethal form of skin cancer [1], and in the advanced-stage disease, defined as unresectable or metastatic melanoma, it is associated

with a poor prognosis [2]. More than 50% melanoma patients harbor mutations in the gene encoding the BRAF kinase [3], a key component of the mitogen-activated protein kinase (MAPK) signaling pathway [3]. The most prevalent mutation, $BRAF^{V600E}$, occurs in the majority of BRAF-mutant cutaneous melanomas and results in a several-hundred-fold increase in kinase activity, leading to constitutive activation of downstream extracellular signal-regulated kinase (ERK) signaling and uncontrolled cellular proliferation [4].

The approval of BRAF inhibitors by the US Food and Drug Administration represents one of the most significant advances in the treatment of BRAF-mutant melanoma [3]. Several BRAF inhibitors, including dabrafenib, vemurafenib, and encorafenib, have demonstrated clinical efficacy after successful clinical trials [5]. Notably, dabrafenib (DAB) nearly doubled progression-free survival compared with the standard-of-care agent dacarbazine in metastatic melanoma [6,7]. Nevertheless, despite these initial benefits, BRAF inhibition fails to produce durable responses due to the rapid emergence of acquired resistance [8].

Melanoma cells are characterized by marked metabolic plasticity. Although BRAF-mutant melanoma cells exhibit a predominantly glycolytic phenotype, the pharmacological inhibition of BRAF signaling induces a metabolic shift toward mitochondrial oxidative phosphorylation (OXPHOS) [9]. For example, treatment with vemurafenib was shown to increase mitochondrial mass, reactive oxygen species (ROS) production, and the mRNA expression of peroxisome proliferator-activated receptor gamma coactivator 1-alpha (PGC1α) [9,10]. The induction of OXPHOS reduces the efficacy of BRAF inhibition, while an elevated PGC1α expression is associated with enhanced mitochondrial biogenesis and stem-like phenotype in melanoma cells [11]. These metabolically driven adaptations are biologically significant and may provide opportunities for the identification of novel therapeutic targets.

Mitochondria possess a remarkable capacity to remodel in order to maintain cellular homeostasis [12]. Mitochondrial dynamics are governed by two complementary processes—fusion and fission—which are essential for preserving mitochondrial function and adaptability [12,13]. These processes play critical roles in cellular energy production via OXPHOS, integration of metabolic pathways, and regulation of apoptosis [13].

Mitochondrial fusion involves the merging of two mitochondria through the coordinated action of three membrane-bound GTPases: mitofusin-1, mitofusin-2, and optic atrophy protein-1 (OPA1) [13,14]. Fusion contributes to the stabilization and restoration of mitochondrial function and has been shown to attenuate chemotherapy-induced apoptosis [14,15]. Conversely, mitochondrial fission results in the division of a single mitochondrion into two smaller organelles [14]. Dynamin-related protein 1 (DRP1) is the principal mediator of mitochondrial fission, functioning in concert with accessory proteins such as fission protein 1 (FIS1) [14], and DRP1 overexpression has been correlated with increased cellular proliferation and chemoresistance across multiple cancer types [16].

In addition, mitophagy—the selective autophagic degradation of mitochondria—can either promote cell survival or enhance therapeutic sensitivity, depending on the cellular context. Specifically, the role of mitophagy is influenced by drug mechanisms of action, cellular energy metabolism, ROS levels, and apoptotic signaling pathways [14]. One key resistance mechanism involves mitophagy-mediated inhibition of apoptosis. In several tumor types, PTEN-induced putative kinase 1 (PINK1)-dependent mitophagy suppresses cytochrome c release and the apoptotic process [14,17]. When mitophagy is activated, PINK1 expression is stabilized at high levels, whereas degradation of mitochondrial import receptor subunit TOM20 homolog (TOM20) serves as a marker of mitophagy [18]. Moreover, certain anticancer agents can modulate mitochondrial dynamics and mitophagy by affecting the stability and activity of the proteins involved in these processes.

Induction of OXPHOS is associated with elevated intracellular ROS levels, as recently demonstrated by Eller et al. in DAB-resistant melanoma cells [19]. However, the pro-tumorigenic or anti-tumorigenic effects of ROS depend on both their intracellular concentration and the antioxidant capacity of the cell. Consequently, therapeutic strategies aimed at targeting antioxidant defense systems in BRAF inhibitor-resistant melanoma cells may represent a promising approach to counteract tumor progression and restore drug sensitivity.

Recently, two human melanoma cell lines were rendered resistant to DAB, and their phenotypes were characterized at the molecular level. In particular, these cell populations were examined for the activation of pro-tumorigenic signaling pathways and their propensity toward cell proliferation or cell death [20]. This study demonstrated that DAB-resistant A375 and FO-1 melanoma cells (A375R and FO-1R), when maintained in the presence of dabrafenib, fully restored high proliferative capacity and exhibited aberrant expression of multiple oncoproteins compared with their DAB-sensitive parental counterparts (A375P and FO-1P) [20].

In the present study, we investigated the effects of the amphibian ribonuclease (RNase) onconase® (ONC; Alfacell Corporation, Somerset, NJ, USA) [21] on both parental and DAB-resistant melanoma cell lines. ONC is a secretory 104 AA residue RNase variant, firstly called ranpirnase, because it is extracted from *Rana pipiens* oocytes. ONC belongs to the pancreatic-type (pt)-RNase superfamily, whose prototype is bovine RNase A [22], because it folds like all pt-RNases (Supplementary Figure S1A) and shares the same His/Lys/His catalytic triad [22,23]. ONC is less active than RNase A versus yeast single-stranded (ss)-RNA [24] but more active versus tRNAs [25], miRNAs [26], and double-stranded (ds)-RNA [27]. Consequently, ONC can also exert antiviral activity [28,29], and, furthermore, it is remarkably cytostatic and cytotoxic against human and mouse leukemic cell lines [30], human glioma [31], lymphoma [32], pancreatic adenocarcinoma [33], and melanoma cell lines [34]. From these results, ONC was also successfully tested in vivo in Phase II and Phase III clinical trials, resulting in activity against non-small-cell lung cancer [35], malignant mesothelioma [36], and displayed synergism with many gold standard drugs for different tumors, either in vitro or in vivo [36]. ONC evades the cellular RNase inhibitor (cRI) [37] that irreversibly blocks most mammalian secretory pt-RNases, since it lacks residues that permit the formation of the pt-RNase–cRI complex [38]. In addition, the ONC highly positively charged surface [39] allows its interaction with the negatively charged membrane of cancer cells [40]. In this way, ONC can be fruitfully and specifically internalized into tumor cells, in turn becoming a promising tool against tumors [41].

In this work, we specifically focused on the putative mechanisms of action of this amphibian RNase, including its ability to modulate ROS levels, antioxidant protein expression, mitochondrial dynamics, mitophagy, lipid peroxidation, and apoptosis. Notably, ONC exhibited enhanced cytostatic and cytotoxic effects in DAB-resistant cell populations, supporting its potential application as a therapeutic strategy to counteract the malignant phenotype associated with resistance to BRAF inhibitors.

2. Results

2.1. Production, Purification, and Catalytic Activity of Recombinant Onconase (ONC)

ONC was expressed in one liter of *E. coli* solution culture, then it was extracted from inclusion bodies, refolded, chromatographed, and concentrated as reported in the Materials and Methods Section. The start Met(−1) was removed by incubating ONC with aminopeptidase from *Aeromonas proteolytica* (AAP), concentrated and re-chromatographed with the preparative SEC column (Supplementary Figure S1A, blue curve). The peak eluted around 210 mL was collected and concentrated, and from the A_{280} value

(Supplementary Figure S1B), the yield was calculated to be about 11 mg. Mass spectrometry analysis confirmed the correct ONC molecular weight given by the cleavage of Met(−1), which, in turn, permits the enzyme to become catalytically active [42].

The enzymatic activity of ONC was spectrophotometrically measured in solution versus yeast RNA at 300 nm, following the protocol of Kunitz [43]. In parallel with RNase A, assays were repeated in triplicate. Each time-course profile was monitored (Supplementary Figure S1C), and the slope of the initial Abs_{300} decrease provided the relative dAbs/dt, in turn normalized to the enzyme amount used: 7.5 µg and 0.25 µg for ONC and RNase A, respectively. From this, the specific activity per mg was calculated as 50.7 ± 3.8 for RNase A and 1.3 ± 0.1 for ONC, i.e., about 39 times less than RNase A. Recalling that ONC activity versus yeast RNA is about 30 times lower than RNase A [24,44], this difference allows to consider recombinant ONC catalytically active, a feature that is mandatory to exert its biological activities [21].

2.2. Effects of ONC on Cell Morphology and Viability

After 48 h of culture, melanoma cells treated with 1 µM ONC and untreated controls were stained with DAPI to assess nuclear number and morphology. Brightfield and DAPI images show untreated A375 and FO1 cells with preserved morphology, while after ONC treatment, the same cells display loss of adhesion and an increased number of rounded cells, indicating compromised membrane integrity (Figure 1, top).

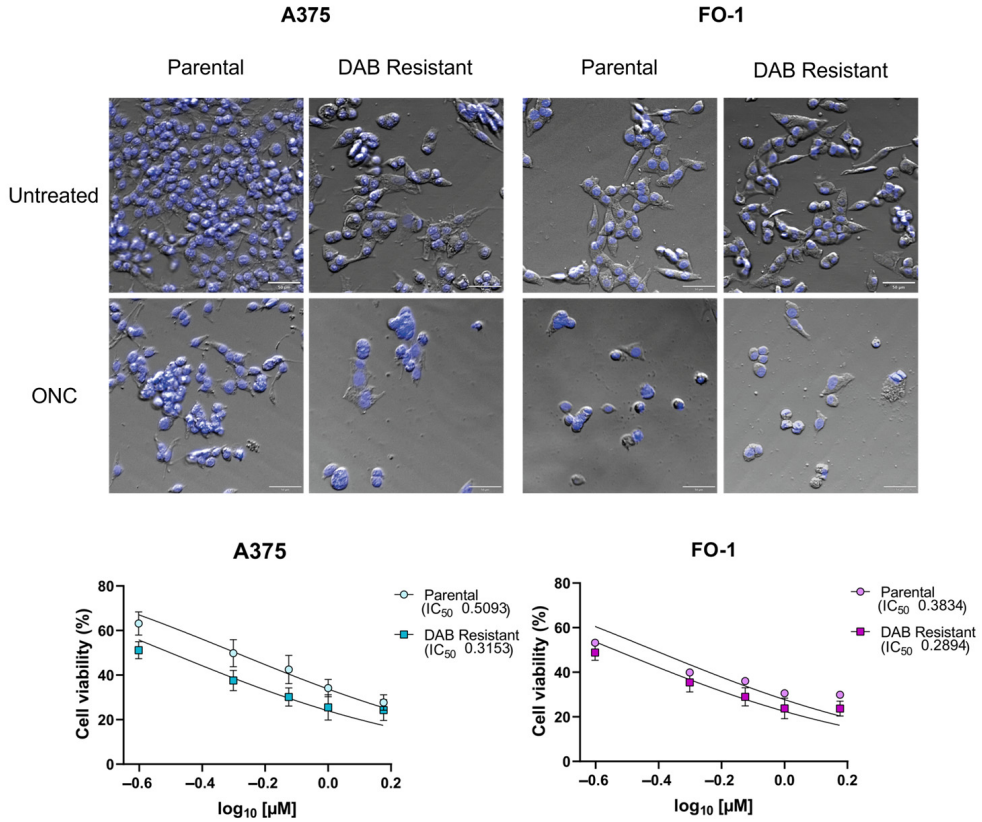

Figure 1. Effects of ONC on cell morphology and viability. (**Top**): Representative images of parental and DAB-resistant A375 and FO1 cell lines. Fluorescence microscopy analysis of A375P, A375R, FO-1P, and FO-1R after 48 h culture in the presence or absence of 1 µM ONC. Cells were fixed with DAPI and analyzed in a fluorescence microscope (Olympus-Evident-Apexview, APX100, Hamburg, Germany). Scale bar: 50 µm. (**Bottom**): The SRB cell viability assay showed a concentration-dependent reduction in cell mass after 72 h of ONC treatment. Calculated IC_{50} values for all cell populations are reported in the figure.

Concurrently, cell viability was quantified using the sulforhodamine B (SRB) assay at different ONC concentrations (0.25, 0.5, 0.75, 1.0, and 1.5 μM). As shown in Figure 1 (bottom), all ONC concentrations induced a highly significant reduction in total cell mass 72 h after ONC treatment. Notably, this effect was more pronounced in DAB-resistant cell populations, as the calculated IC_{50} values were higher in parental than in DAB-resistant cells. In detail, A375P ≈ 0.51 μM; A375R ≈ 0.32 μM; FO-1P ≈ 0.38 μM; and FO-1R ≈ 0.29 μM ONC (see Figure 1).

2.3. ONC Increases Intracellular ROS Levels, Particularly in Dabrafenib-Resistant Melanoma Cell Lines

Parental A375 (A375P) and FO-1 (FO-1P), as well as DAB-resistant A375 (A375R) and FO-1 (FO-1R) melanoma cells, were treated with 1 μM ONC or left untreated for 48 h. Intracellular ROS levels were then assessed by flow cytometry in viable cells after staining with the CellROX Deep Red probe. While no significant differences in ROS levels were observed between untreated and ONC-treated parental cells, ONC treatment induced a significant increase in ROS levels in both A375R and FO-1R cell populations (Figure 2, top).

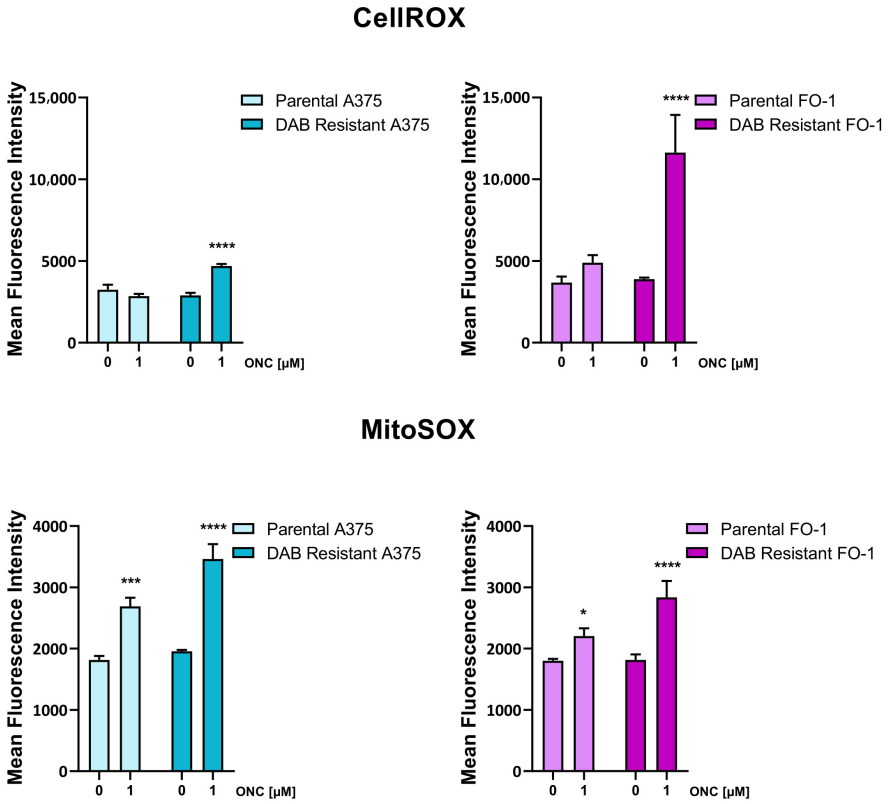

Figure 2. Intracellular levels of reactive oxygen species (ROS). CellROX: Histograms show total intracellular ROS levels in melanoma cell populations treated with 1 μM ONC for 48 h. Upon staining with the CellROX™ Deep Red probe, samples were analyzed in a BD LSRFortessa flow cytometer (BD Biosciences). MitoSOX assay was performed in all melanoma cell populations treated or not with 1 μM ONC for 48 h. Upon staining with MitoSOX, samples were analyzed in a BD LSRFortessa flow cytometer (BD Biosciences). Both total ROS and mitochondrial ROS levels were quantified within the viable cell population. Data represent at least three independent biological replicates. ANOVA test, * $p < 0.05$, *** $p < 0.001$, and **** $p < 0.0001$.

The MitoSOX assay, which is widely used to detect mitochondrial superoxide production, was also performed. After 48 h of ONC treatment, mitochondrial ROS levels were significantly increased in all cell lines. The highest increases in MitoSOX fluorescence were observed in the DAB-resistant cell populations (Figure 2, bottom).

2.4. ONC Reduces the Expression Levels of Antioxidant Proteins

Immunoblotting analyses were performed after 24 or 48 h of cell treatment with 0.5 or 1 μM ONC, to determine the ONC effects on the expression of proteins involved in ROS detoxification.

The nuclear factor erythroid 2–related factor 2 (NRF2) is a central regulator of cellular antioxidant defense, functioning as a master transcription factor that induces the expression of a broad range of antioxidant and cytoprotective proteins [45].

Immunoblotting analyses performed after 24 h of ONC treatment revealed a significant reduction in the expression of the phosphorylated, active form of NRF2 (pNRF2) in all cell populations, except for A375P cells. Consistent with this finding, the expression of heme oxygenase-1 (HO-1), an antioxidant enzyme transcriptionally induced by NRF2, was reduced in the DAB-resistant cell populations (Figure 3, 24 h, and Supplementary Figure S2).

DNA damage was assessed by evaluating the phosphorylation status of histone H2AX (γ-H2AX), a marker of double-strand breaks that may also reflect apoptotic DNA fragmentation [46]. Significant increases in γ-H2AX expression levels were observed in A375P, FO-1P, and FO-1R cell populations after 24 h ONC treatment, indicating the presence of DNA damage and/or activation of DNA repair mechanisms (Figure 3, 24 h, and Supplementary Figure S2). In contrast, the expression levels of other analyzed proteins—including ferroptosis suppressor protein 1 (FSP1), glutamate–cysteine ligase modifier subunit (GCLM), cystine/glutamate transporter (SLC7A11), glutathione S-transferase P1 (GSTP1), glutathione reductase, ferritin heavy chain (FTH1), and mitochondrial superoxide dismutase 2 (SOD2)—did not show significant differences between untreated and ONC-treated cells at this time point (Figure 3, 24 h and Supplementary Figure S2).

After 48 h, ONC markedly reduced the expression levels of pNRF2 and HO-1 in a concentration-dependent manner. In A375P cells, HO-1 expression levels were very low in both untreated and ONC-treated cells (Figure 3, 48 h). The expression levels of GCLM and SLC7A11, both involved in glutathione biosynthesis, as well as GSTP1 and SOD2, were reduced by ONC, at least in the DAB-resistant cell populations (Figure 3, 48 h). In contrast, glutathione reductase expression remained unchanged.

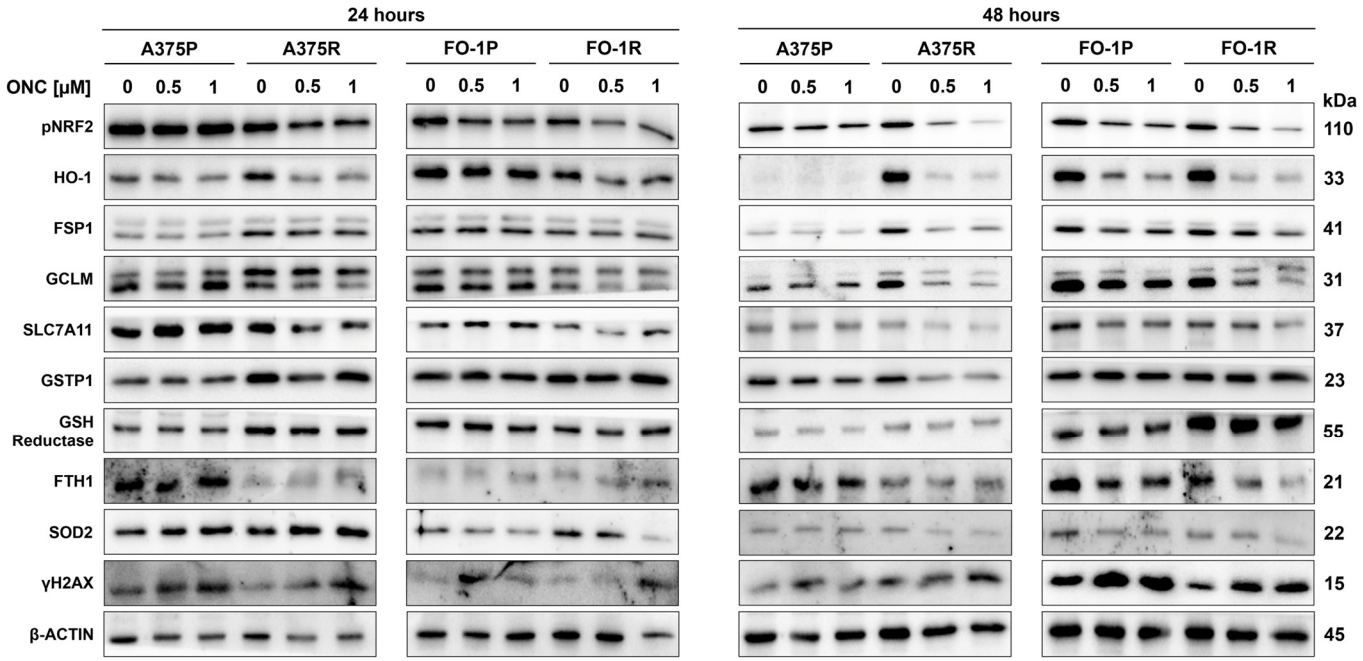

Figure 3. *Cont.*

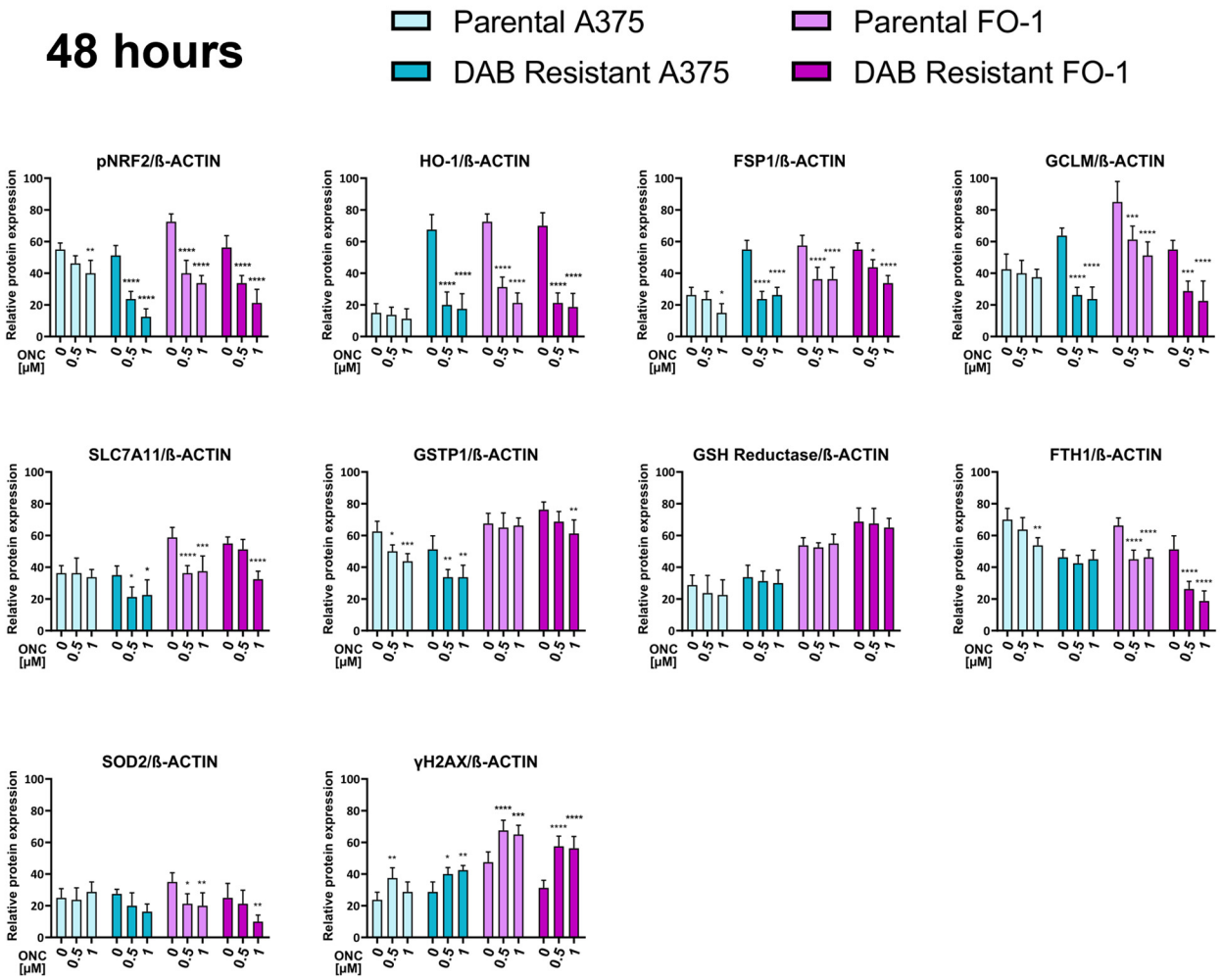

Figure 3. Effects of ONC on the expression of proteins involved in antioxidant defense. A375P, A375R, FO-1P, and FO-1R melanoma cell populations were cultured for 24 h (**left**) or 48 h (**right**) in the presence or absence of 0.5 or 1 μM ONC. (**Top**): Immunoblots showing the expression levels of phosphorylated nuclear factor erythroid 2–related factor 2 (pNRF2), heme oxygenase-1 (HO-1), ferroptosis suppressor protein 1 (FSP1), glutamate–cysteine ligase modifier subunit (GCLM), cystine/glutamate transporter (SLC7A11), glutathione S-transferase P1 (GSTP1), glutathione reductase, ferritin heavy chain (FTH1), mitochondrial superoxide dismutase 2 (SOD2), and the phosphorylated form of histone H2AX (γ-H2AX). (**Bottom**): Histograms showing mean protein expression levels at 48 h, ±S.D., determined by densitometric analysis deriving from three independent experiments. Histograms of different protein expression levels registered after 24 h of ONC treatment are shown in Supplementary Figure S2. All comparisons were performed relative to the corresponding control samples, after normalization to β-actin expression; ANOVA test: * $p < 0.05$, ** $p < 0.01$, *** $p < 0.001$, and **** $p < 0.0001$.

Notably, ONC-treated cells exhibited a reduced expression level of FSP1, an enzyme that catalyzes the reduction of oxidized ubiquinone to ubiquinol and acts as a potent lipophilic antioxidant, thereby preventing the propagation of membrane lipid peroxidation [47]. Ferritin expression was partially affected by ONC treatment, especially in the FO-1 cell populations (Figure 3, 48 h). Finally, evidence of DNA damage and/or activation of DNA repair mechanisms, as indicated by increased γ-H2AX expression, was observed in all cell populations (Figure 3, 48 h).

2.5. ONC Modulates the Expression of Proteins Involved in Mitochondrial Biogenesis, and Dynamics

The generation of ROS occurs predominantly at the electron transport chain located on the inner mitochondrial membrane during cellular respiration. Accordingly, we investigated whether ONC affects key mitochondrial dynamics, including biogenesis, and fusion/fission.

Peroxisome proliferator-activated receptor gamma coactivator 1-alpha (PGC-1α) is a master regulator of mitochondrial biogenesis, and its expression has been associated with a more malignant phenotype in melanoma [11]. Immunoblotting analyses revealed slight differences between ONC-treated and untreated cells in the expression of PGC1α, indicating that, within the first 24 h, ONC significantly decreased mitochondrial biogenesis only in the FO-1P cell population (Figure 4, 24 h, and Supplementary Figure S3). In addition, OPA1 protein levels were slightly reduced exclusively in DAB-resistant cell populations. Conversely, the expression levels of mitofusin-1 and mitofusin-2 remained unchanged (Figure 4, 24 h, and Supplementary Figure S3). Total DRP1 protein and its active phosphorylated form (pSer616-DRP1) levels were decreased mainly in the A375 cell line, whereas FIS1 expression was reduced in the FO-1R cell population (Figure 4, 24 h, and Supplementary Figure S3), suggesting that mitochondrial fission starts being affected by ONC early on.

Previous studies have reported that downregulation of the c-Myc oncogene leads to a progressive reduction in mitochondrial mass and accelerated loss of mitochondrial membrane potential [48,49]. Consistently, our data showed that ONC significantly reduces c-Myc expression in all cell lines except A375P within 24 h of treatment (Figure 4, 24 h, and Supplementary Figure S3).

Finally, we evaluated the expression level of three mitochondrial inner membrane proteins, ubiquinol–cytochrome c reductase core protein 1 (UQCRC1, complex I), cytochrome c oxidase subunit IV (COX4, complex IV), and ATP synthase subunit β (ATP5B, complex V), along with a cytosolic enzyme used as a loading control, glyceraldehyde-3-phosphate dehydrogenase (GAPDH). None of these proteins showed significant changes in expression following 24 h ONC treatment, suggesting that they are not directly affected early on.

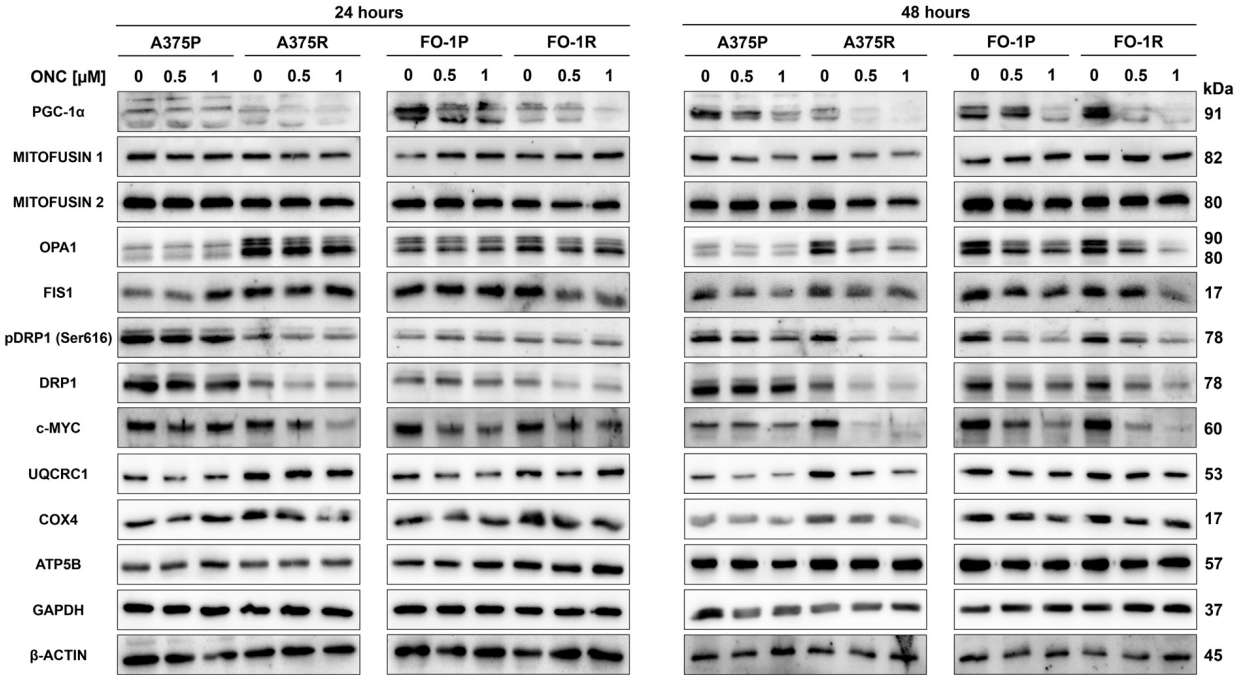

Figure 4. *Cont.*

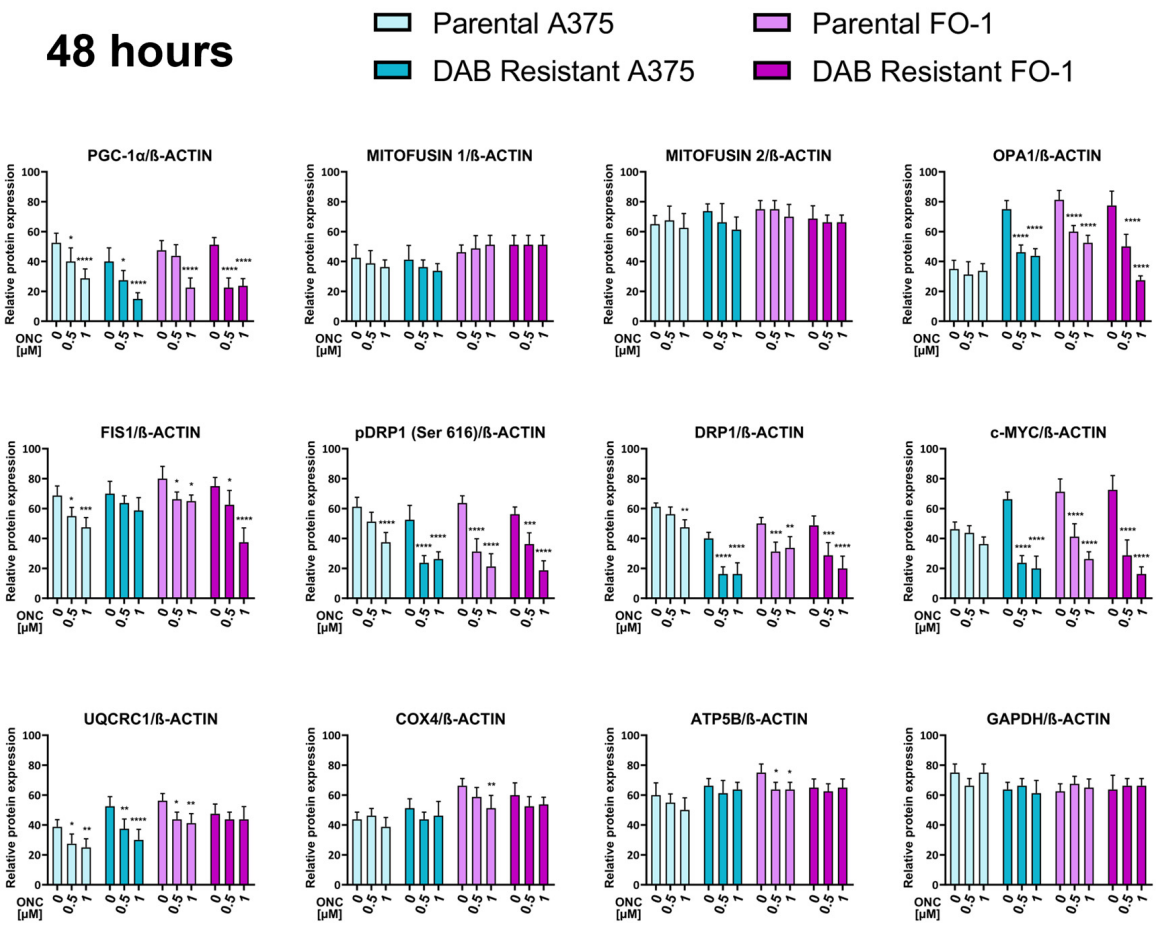

Figure 4. Effects of ONC on the expression of proteins involved in mitochondrial biogenesis and dynamics. A375P, A375R, FO-1P, and FO-1R melanoma cell populations were cultured for 24 h (**left**) or 48 h (**right**) in the presence or absence of 0.5 or 1 μM ONC. (**Top**): Representative immunoblots showing the expression levels of peroxisome proliferator-activated receptor gamma coactivator 1-α (PGC-1α), optic atrophy protein 1 (OPA1), mitofusin-1 and mitofusin-2, dynamin-related protein-1 (DRP1), fission protein-1 (FIS1), the oncogene c-Myc, ubiquinol–cytochrome c reductase core protein 1 (UQCRC1), cytochrome c oxidase subunit IV (COX4), ATP synthase subunit β (ATP5B), and glyceraldehyde-3-phosphate dehydrogenase (GAPDH). (**Bottom**): Histograms reporting mean protein expression levels at 48 h, ±S.D., determined by densitometric analysis deriving from three independent experiments. (Histograms of different protein expression levels obtained after 24 h of ONC treatment are shown in Supplementary Figure S3.) All comparisons were performed relative to the corresponding control samples after normalization to β-actin expression; ANOVA test: * $p < 0.05$, ** $p < 0.01$, *** $p < 0.001$, and **** $p < 0.0001$.

Overall, after 48 h of ONC treatment, differences between treated and untreated cells became more pronounced. PGC1α expression was significantly reduced across all cell populations, whereas OPA1 expression significantly decreased in all cells except A375P ones. However, the expression levels of mitofusin-1 and mitofusin-2 remained unaltered (Figure 4, 48 h), consistent with the results obtained after 24 h. Regarding proteins involved in mitochondrial fission, both total DRP1 and p(Ser616)-DRP1 levels were significantly reduced, and FIS1 expression also slightly decreased (Figure 4, 48 h).

Collectively, these findings indicate a diminished ability of ONC-treated cells to sustain mitochondria biogenesis and to divide mitochondria into smaller organelles. Conversely, the impact of ONC on mitochondrial fusion is difficult to interpret due to reduced OPA1 expression alongside largely unchanged mitofusin-1 and mitofusin-2 levels.

Consistent with the 24 h time point, the expression levels of COX4, ATP5B, and the glycolytic enzyme GAPDH remained unchanged at 48 h (Figure 4, 48 h). In contrast, the expression level of the complex I protein UQCRC1 was significantly decreased in all cell populations except FO-1R cells (Figure 4, 48 h), suggesting that ONC may mildly compromise the electron transport chain at this time point.

2.6. ONC Induces Mitochondria Shape Elongation

Given the alterations observed in the expression of proteins regulating mitochondrial biogenesis and fission/fusion dynamics, we next investigated whether ONC treatment also affected mitochondrial morphology. To this end, mitochondrial structure was analyzed by MitoTracker Green staining following 48 h of ONC exposure.

MitoTracker Green staining revealed differences in mitochondrial morphology between cells treated with 1 μM ONC for 48 h and untreated cells from the same populations. In particular, ONC-treated cells exhibited more elongated mitochondria than untreated ones. This elongation was consistently observed across all analyzed cell lines (A375 and FO-1), but it was more pronounced in the DAB-resistant A375 cell population (Figure 5).

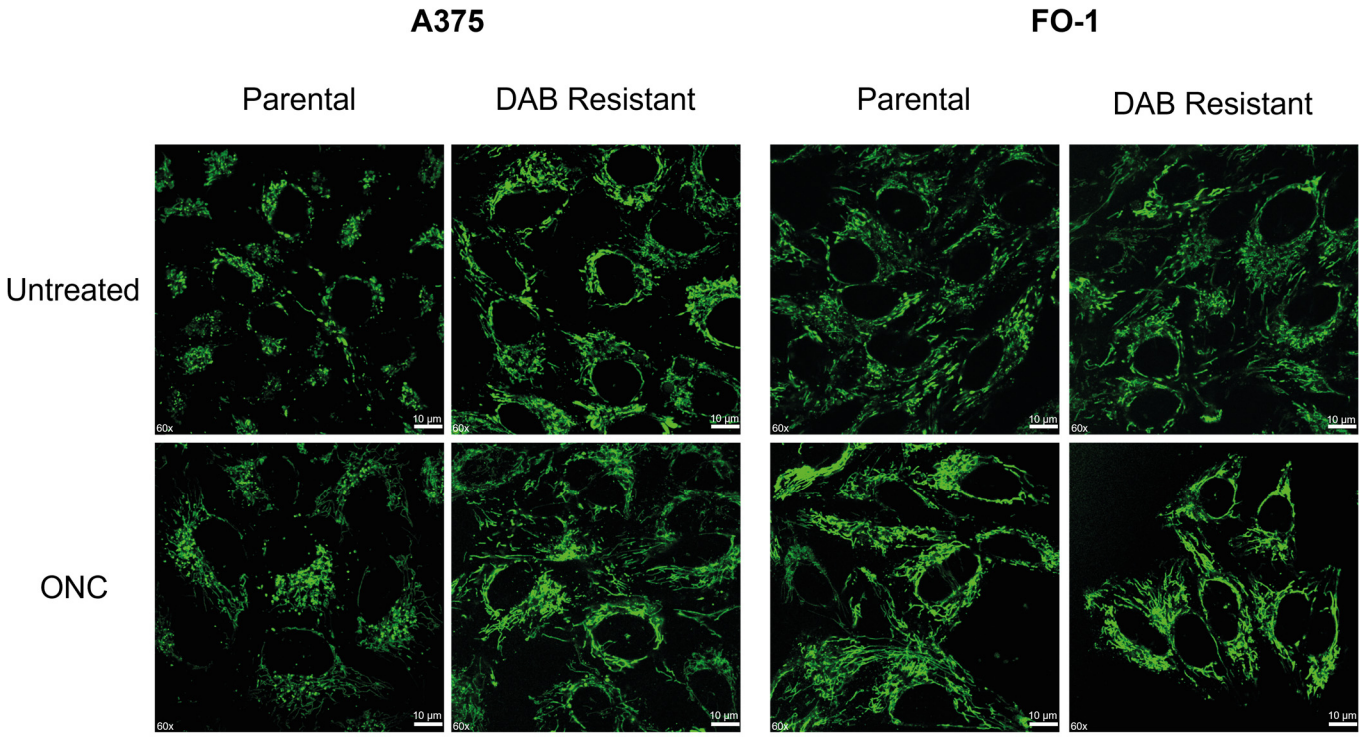

Figure 5. Representative images of mitochondrial staining with MitoTracker Green FM in parental and DAB-resistant A375 and FO-1 cell lines. Control cells are shown in the top panel, while the corresponding cell lines treated with 1 μM ONC are shown in the bottom panel. All images were acquired using an Evident FV4000 confocal microscope (Olympus, Milan, Italy) at 60× magnification (1.4 NA) oil immersion. After acquisition, all images were deconvolved using the Scientific Volume Imaging software (v18.10, Hilversum, The Netherlands. Scale bar: 10 μm).

2.7. ONC Modulates the Expression of Proteins Involved in Cell Proliferation and Cell Death

It is well established that ONC disrupts multiple signaling pathways that support the high proliferative capacity of melanoma cells [34,50,51]. In light of the pronounced effects of ONC on mitochondrial homeostasis and redox balance, particularly in the two DAB-resistant melanoma cell lines, we next investigated whether alterations in pathways regulating cell proliferation and cell death were also maintained in DAB-resistant cell populations. Signal Transducer and Activator of Transcription 3 (STAT3) and nuclear

factor kappa-light-chain-enhancer of activated B cells (NF-κB) are transcription factors that regulate the expression of numerous genes in response to cellular stimuli and play crucial roles in processes like cell growth and apoptosis [52–54]. After 24 h of ONC treatment, the expression levels of phosphorylated STAT3 (Tyr705) and phosphorylated NF-κB p65 subunit were significantly reduced in all cell lines, except A375P (Figure 6, 24 h, and Supplementary Figure S4). In contrast, ERKs, which act downstream of BRAF signaling, showed no changes in either total protein levels or phosphorylated (active) forms. Similarly, the expression of two markers of cell proliferation, the active forms of cyclin-dependent kinases 2 and 4 (pCDK2 and pCDK4), did not significantly change within the first 24 h of treatment (Figure 6, 24 h, and Supplementary Figure S4). The expression levels of the phosphorylated form of cyclin-dependent kinase1 (pCDK1) were also evaluated because active CDK1 phosphorylates DRP1 on Ser 616 [55]. Interestingly, pCDK1 expression levels decreased in FO-1R cells at this time (Figure 6, 24 h, and Supplementary Figure S4).

As a marker of apoptosis, the expression of the cleaved form of poly (ADP-ribose) polymerase-1 (cleaved PARP) was analyzed by immunoblotting. Cleaved PARP expression levels increased in nearly all cell lines, indicating an early activation of apoptotic processes. Apoptosis is tightly regulated by a balance between pro- and anti-apoptotic proteins, including survivin, a member of the inhibitors of apoptosis protein family. Survivin inhibits caspase activation and thereby negatively regulates apoptosis in several tumor types, including melanoma [56,57]. Our results revealed a slight reduction in survivin expression in FO-1R cells after 24 h of ONC treatment (Figure 6, 24 h, and Supplementary Figure S4).

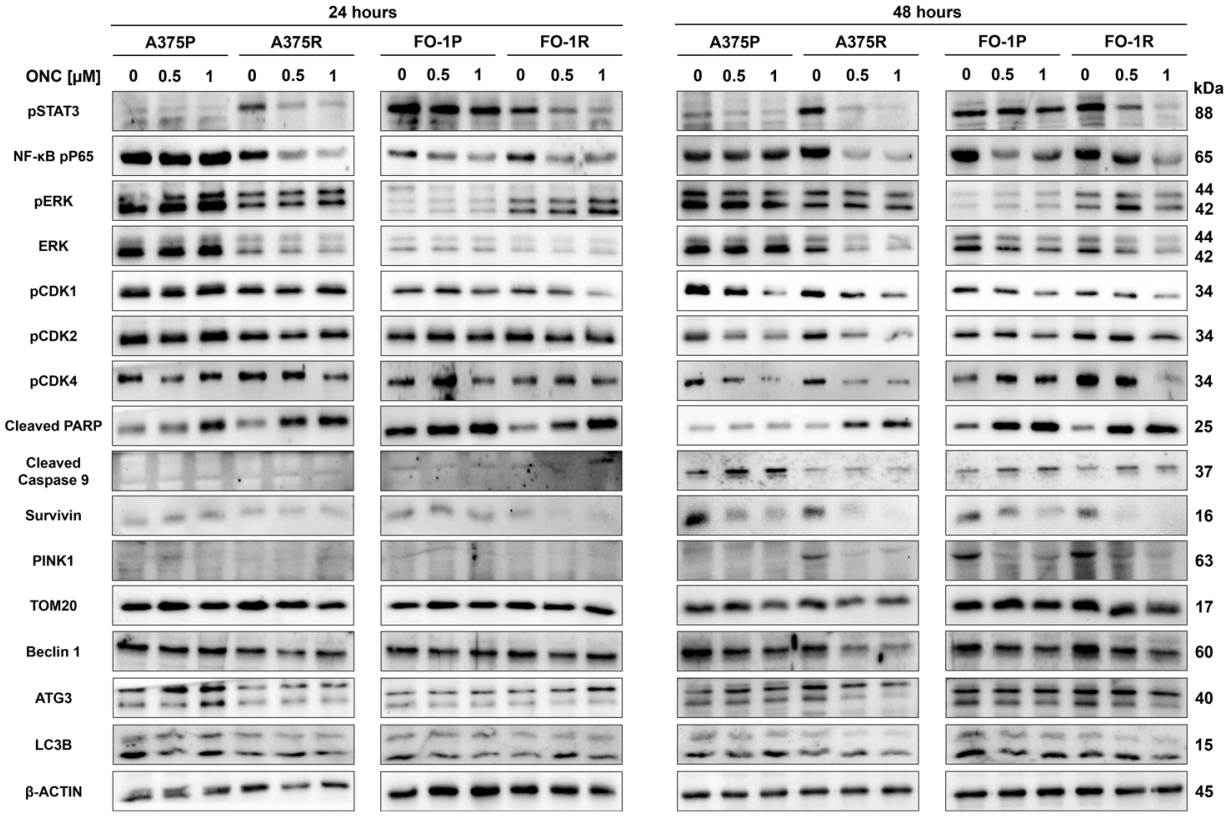

Figure 6. *Cont.*

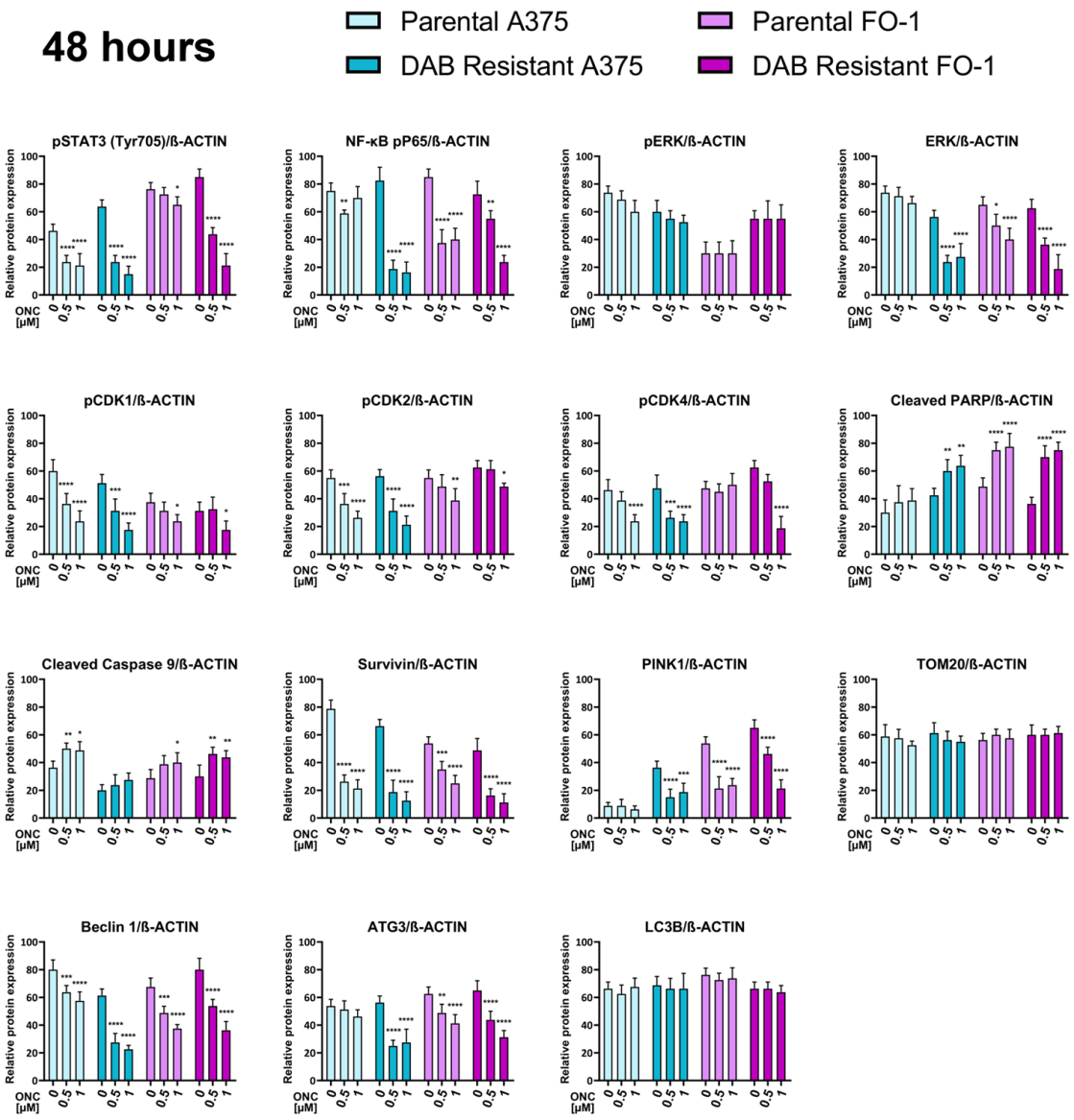

Figure 6. Effects of ONC on the expression of proteins involved in cell proliferation and cell death. A375P, A375R, FO-1P, and FO-1R melanoma cell populations were cultured for 24 h (**left**) or 48 h (**right**) in the presence or absence of 0.5 or 1 μM ONC. (**Top**): Representative immunoblots showing the expression levels of the phosphorylated forms of Signal Transducer and Activator of Transcription 3 (pSTAT3) and nuclear factor kappa-light-chain-enhancer of activated B cells (pP65-NF-κB), the phosphorylated and total forms of extracellular signal-regulated kinase (pERK and ERK), the phosphorylated forms of cyclin-dependent kinases 1, 2, and 4 (pCDK1, pCDK2 and pCDK4), cleaved poly(ADP-ribose) polymerase-1 (cleaved-PARP), cleaved caspase-9, survivin, PTEN-induced putative kinase 1 (PINK1), mitochondrial import receptor subunit TOM20 homolog (TOM20), Beclin1, Autophagy Related 3 (ATG3), and microtubule-associated protein 1 light chain 3 beta (LC3B). (**Bottom**): Histograms showing mean protein expression levels after 48 h ONC treatment ± S.D., as determined by densitometric analysis from three independent experiments. Histograms of different protein expression levels obtained after 24 h of ONC treatment are shown in the Supplementary Figure S4. All comparisons were performed relative to the corresponding control samples after normalization to β-actin expression; ANOVA test: * $p < 0.05$, ** $p < 0.01$, *** $p < 0.001$, and **** $p < 0.0001$.

Finally, we assessed whether ONC induces autophagy, with particular attention to mitophagy. PTEN-induced putative kinase 1 (PINK1) is activated by autophosphorylation and accumulates on the outer mitochondrial membrane of dysfunctional mitochondria,

triggering a signaling cascade that culminates in mitochondrial sequestration by autophagosomes [58]. PINK1 expression was very low in either untreated or treated cells with ONC for 24 h (Figure 6, 24 h, and Supplementary Figure S4). TOM20 is an outer mitochondrial membrane protein that collaborates with PINK1 in mitophagy, and degradation of TOM20 occurs prior to mitophagy [18]. In our experimental model, TOM20 expression levels were not affected by ONC treatment (Figure 6, 24 h, and Supplementary Figure S4). Beclin1 and Autophagy Related 3 (ATG3) are proteins involved in the initiation and maturation of autophagosomes [59]. Both proteins were constantly expressed at 24 h either in the presence or in the absence of ONC (Figure 6, 24 h, and Supplementary Figure S4). Finally, no evidence of different expression of microtubule-associated protein 1 light chain 3 beta (LC3B) was detected (Figure 6, 24 h, and Supplementary Figure S4).

After 48 h of treatment, ONC continued to suppress the active forms of STAT3 and NF-κB (pSTAT3 and pP65 NF-κB). Total ERK protein levels were reduced in all cell lines except A375P, whereas phosphorylated ERK (pERK) levels were not affected by ONC treatment (Figure 6, 48 h). At this time point, cell proliferation appeared to be impaired, as indicated by a significant reduction in the active forms of CDK2 and CDK4 (pCDK2 and pCDK4). Additionally, the active form of CDK1 (pCDK1) was decreased in all cell lines (Figure 6, 48 h), consistent with the p(Ser616)-DPR1 downregulation at the same time point (Figure 4, 48 h).

In agreement with the 24 h treatment findings, apoptosis remained prominent, as demonstrated by increased levels of both cleaved PARP and cleaved caspase-9, whereas the antiapoptotic survivin was markedly downregulated following 48 h of ONC treatment in all cell populations (Figure 6, 48 h). Although PINK1 expression became detectable after 48 h of culture in untreated cells, it was strongly reduced by ONC treatment, while TOM20 expression was not significantly lowered. Moreover, Beclin1 and ATG3 expressions were reduced, whereas LC3B expression levels remained unaltered. Overall, these findings suggest that ONC does not induce either mitophagy or autophagy (Figure 6, 48 h).

2.8. ONC Effects on Autophagosomes Formation, Lipid Peroxidation, and Apoptotic Cell Death

The monodansylcadaverine (MDC) assay was performed in untreated cell populations or after 48 h of ONC treatment. MDC fluorescence was slightly increased in the A375P cell line, whereas no detectable increase in autophagosome formation was observed in the other cell populations (Figure 7, top panel). These results indicate that ONC has, at most, a marginal effect on autophagy, consistent with the immunoblot data.

Lipid peroxidation was assessed exploiting the BODIPY-C11 assay. Flow cytometry analysis revealed an increase in lipid peroxidation in A375P and A375R cell populations, whereas only a modest but significant increase was observed in FO-1R cells (Figure 7, top panel).

Finally, apoptotic cell death was evaluated using the Annexin V/propidium iodide (PI) assay in untreated or 48 h ONC-treated cell populations. ONC treatment significantly increased the percentage of Annexin V- and/or PI-positive cells in all cell populations. Differences between untreated and ONC-treated cells were more evident in the A375 cell line, since FO-1 cell populations present higher basal levels of apoptosis (Figure 7, bottom panel).

Immunoblot analysis was also performed in the presence or absence of the caspase inhibitor Z-VAD-FMK (25 μM). In all cell populations, the ONC-dependent induction of cleaved PARP expression was partially reversed by Z-VAD-FMK pretreatment, confirming that ONC-induced cell death occurs, at least in part, through a process elicited by caspases (Figure 7, bottom panel).

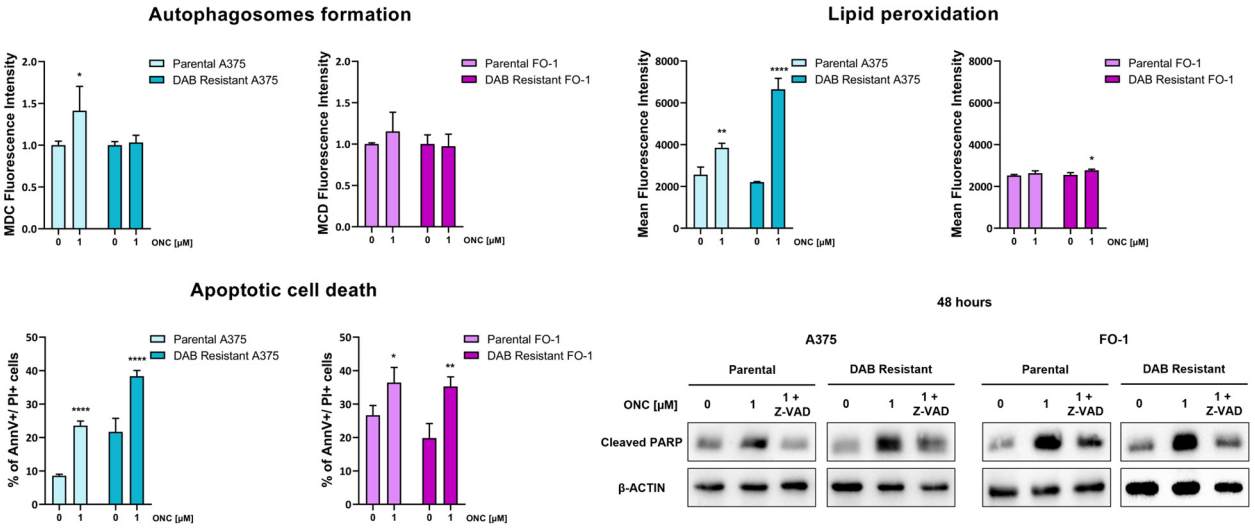

Figure 7. ONC effects on cell death. A375P, A375R, FO-1P, and FO-1R were untreated or ONC-treated for 48 h. (**Top** (**left**)): MDC fluorescence was measured using a microplate reader and normalized to cell mass by crystal violet assay. (**Top** (**right**)): Lipid peroxidation was quantified by BODIPY-C11 assay. Flow cytometry analysis was performed using a BD LSRFortessa flow cytometer. Fluorescence signals were quantified within the total cell population of each cell line. (**Bottom** (**left**)): Cells were stained with Annexin V–FITC and propidium iodide (PI). Flow cytometry analysis was performed using a BD LSRFortessa instrument. (**Bottom** (**right**)): Cells were pre-treated or not with 25 μM Z-VAD-FMK and subsequently treated with 1 μM ONC. Immunoblot analysis showed increased expression levels of cleaved PARP, while Z-VAD_FMK pre-treatment partially reverted this increase. Data were normalized with β-actin expression levels. ANOVA test: * $p < 0.05$, ** $p < 0.01$, and **** $p < 0.0001$.

3. Discussion

The therapeutic management of advanced melanoma remains challenging, as this malignancy exhibits poor responsiveness to conventional chemotherapy and radiotherapy [60]. Over the past decade, however, the 5-year survival rate has significantly improved with the introduction of targeted therapies, including BRAF and MEK inhibitors, as well as immunotherapeutic approaches [61]. Despite these advances, acquired resistance frequently develops within approximately one year of treatment initiation [8].

As a potential novel therapeutic strategy against melanoma, we had previously investigated the antitumor effects of onconase (ONC), an amphibian ribonuclease accompanied by cytotoxic activity in mammalian cells, using melanoma cell models. Our previous findings showed that ONC selectively reduces melanoma cell viability while sparing normal human epidermal melanocytes. Moreover, ONC impairs NF-κB DNA binding and the expression of its downstream target tumor necrosis factor-α (TNF-α), and it attenuates cell migration, invasion, colony formation, and matrix metalloproteinase-2 activity in BRAF-mutated melanoma cell lines [34,62]. We further compared the biological effects of monomeric and dimeric ONC in both BRAF-mutated and BRAF-wild-type melanoma cells [50]. Finally, we demonstrated that ONC induces the upregulation of miR-20a-3p, miR-29a-3p, and miR-34a-5p, accompanied by the downregulation of several proteins targeted by these microRNAs [51].

In the present study, we investigated the mechanisms underlying ONC-induced cytotoxicity in two BRAF-mutated melanoma cell lines that are either sensitive or resistant to dabrafenib (DAB), focusing on its effects on antioxidant protein expression, ROS production, and the regulation of mitochondrial dynamics.

In cancer, ROS production can exert either pro-tumorigenic or anti-tumorigenic effects. Oxidative stress arises from an imbalance between the ROS production and the ability of biological systems to detoxify these highly reactive molecules, or to repair the damage they induce [45]. Despite elevated ROS levels, melanoma cells maintain redox homeostasis through adaptive alterations in bioenergetic metabolism, thereby acquiring high antioxidant capacity. This adaptation involves upregulation of the pentose phosphate pathway, increased expression of antioxidant defense proteins, modulation of mitochondrial metabolism, and other mechanisms [63].

Several genes participate in ROS detoxification by buffering oxidative stress and preserving redox balance in cancer cells [64]. This antioxidant response is primarily controlled by the transcription factor NRF2, a master regulator of cytoprotective and antioxidant gene expression, which can provide melanoma cells with a survival advantage under conditions of oxidative stress. Consistently, a high nuclear NRF2 expression in melanoma patients has been associated with significantly poorer survival outcomes [65]. NRF2 regulates the expression of multiple antioxidant effectors, including enzymes involved in the glutathione antioxidant system (GCLM, SLC7A11, glutathione transferase P1, and glutathione peroxidases). Heme oxygenase-1 (HO-1) is another NRF2-regulated antioxidant enzyme that catalyzes heme degradation, generating antioxidant biliverdin and carbon monoxide, along with the pro-oxidant ferrous iron [66]. The dual role of HO-1 in cancer appears to depend on the presence of iron-scavenging molecules, in particular ferritin, which sequesters intracellular free iron within its cages [66]. NRF2 also induces the expression of all superoxide dismutase (SOD) isoenzymes, including mitochondrial SOD2, which is particularly relevant given the elevated ROS production in mitochondria [67]. Notably, BRAF-mutated melanoma cells adapt to BRAF inhibition by increasing SOD2 expression [68]. Remarkably, increased NRF2 expression has been frequently observed in several types of chemoresistant cancer cells [67,69].

In our melanoma cell model, ONC treatment led to a marked reduction in the expression of the active form of NRF2 and its major downstream target, HO-1 (Figure 3). After 48 h treatment, several additional antioxidant proteins—GCLM, SLC7A11, GSTP1, FSP1, and SOD2—were also significantly downregulated. Notably, the genes encoding these proteins are transcriptional targets of NRF2, suggesting that ONC-induced cytotoxicity may be mediated, at least in part, through suppression of NRF2-dependent antioxidant defenses. This interpretation is supported by the pronounced ONC-induced elevation in mitochondrial superoxide. Elevations in both total and mitochondrial ROS were more evident in DAB-resistant cell lines following ONC treatment (Figure 2). These results are consistent with ONC's capacity to overcome the heightened antioxidant defenses characteristic of DAB-resistant melanoma cells. Accordingly with this latter notion, Eller et al. reported that DAB-resistant A375 cells exhibit a more efficient antioxidant system, explaining why, despite ongoing cell death, a net increase in cell growth was observed [19]. These initial observations prompted us to further investigate mitochondrial function, with particular emphasis on mitochondrial biogenesis, dynamics, and mitophagy.

PGC1α is a key transcriptional regulator of mitochondrial biogenesis [10,11]. Notably, PGC1α-positive melanoma cells have been reported to display enhanced mitochondrial oxidative metabolism and increased ROS detoxification capacity, which supports their survival under oxidative stress conditions. In contrast, PGC1α-negative melanoma cells are more glycolytic and exhibit heightened sensitivity to ROS-inducing agents [70]. Our experiments demonstrated a marked reduction in PGC1α expression at 48 h following ONC treatment in both DAB-sensitive and -resistant melanoma cell populations (Figure 4). The timing of this downregulation is consistent with the observed increase in ROS levels and the concomitant decrease in major antioxidant-related proteins, as described below.

Indeed, we previously reported that ONC requires a latency period of 1–2 days to exert its cytostatic and cytotoxic effects in melanoma cells [34,51].

The balance between mitochondrial fission and fusion both reflects and regulates mitochondrial metabolism and apoptosis [13]. DRP1, a principal mediator of mitochondrial fission, was downregulated after 24 h of ONC treatment in the DAB-resistant subsets of melanoma cells. This effect became more pronounced at 48 h following ONC administration, a time-point at which both DAB-sensitive and -resistant melanoma cells exhibited reduced expression of DRP1 as well as its active, phosphorylated form (Figure 4). These findings were accompanied by decreased expression of FIS1, another protein involved in mitochondrial fission. The oncogene c-Myc is known to exert substantial control over mitochondrial dynamics through the transcriptional regulation of DRP1 [71]. Immunoblot analyses revealed a marked reduction in c-Myc expression across all cell lines except A375P cells (Figure 4), suggesting a potential mechanism underlying DRP1 downregulation. In addition, ONC treatment led to reduced pCDK1 levels (Figure 6), which may further promote DRP1 inactivation. Notably, CDK1 acts as an upstream kinase that phosphorylates DRP1 at serine 616, thereby enhancing its activity [55].

Mitochondrial fragmentation facilitates the segregation of damaged mitochondrial components, targeting them for removal through mitophagy [71]. Our data indicate that ONC impairs not only mitochondrial fission but also mitophagy. Specifically, PINK1, a key initiator of mitophagy [72], was significantly downregulated, while TOM20 expression remained unchanged following ONC exposure (Figure 6). Furthermore, levels of ATG3—an autophagosome maturation-related protein—were decreased by ONC in all cell lines except A375P, and LC3B levels did not increase at any time-point following ONC treatment (Figure 6). Finally, no significant increase in autophagosome formation was assessed using the monodansylcadaverine assay after ONC treatment, with the exception of A375P cells (Figure 7).

Mitochondrial fusion allows the organelle to mitigate the detrimental effects of genetic dysfunction [13]. A previous study reported that the BRAF inhibitor vemurafenib induces a hyperfused mitochondrial phenotype and enhances oxidative phosphorylation, thereby promoting melanoma resistance [73]. Mitochondrial fusion is primarily regulated by mitofusin-1, mitofusin-2, and OPA1. Under our experimental conditions, ONC did not alter the expression of mitofusin-1 or mitofusin-2, whereas OPA1 expression was reduced, particularly in DAB-resistant cells (Figure 4). To determine whether mitochondrial fission/fusion was detectable, cells were stained with MitoTracker Green and analyzed by confocal microscopy. ONC-treated cells displayed more elongated mitochondria (Figure 5), indicating that the predominant effect of ONC is inhibition of mitochondrial fission, resulting in mitochondrial elongation, despite the reduction in OPA1 protein levels.

In summary, our findings suggest that ONC inhibits several processes involved in mitochondrial plasticity, including mitochondrial biogenesis, fission, and mitophagy. As a consequence, mitochondria become more vulnerable to irreversible damage, as evidenced by increased γ-H2AX expression and induction of apoptosis.

Finally, we investigated the ability of ONC to modulate selected proliferation signaling pathways, cell cycle–related proteins, and cell death. We observed a marked reduction in the active forms of STAT3 and the NF-κB P65 subunit in both DAB-sensitive and -resistant cell populations (Figure 6), with these effects being more pronounced in DAB-resistant cells (Figure 6). Although the phosphorylated forms of ERK were unaffected, the total ERK levels decreased 48 h after ONC treatment (Figure 6). The reduced total ERK protein levels may be explained by ONC-mediated increased expression of miR-20a, miR-29a, and miR-34a. MAPK1, which encodes ERK2, is a validated target of all three microRNAs, which are highly expressed in A375P and FO-1P cell lines following ONC treatment, as

previously reported [51]. These findings are consistent with a concomitant reduction in cell proliferation, as also evidenced by a decreased expression of both active forms of CDK1, CDK2, and CDK4 (Figure 6).

With respect to cell death, our data do not support the induction of autophagy or mitophagy, as discussed above. Ferroptosis activation in melanoma is tightly linked to increased lipid peroxidation and suppression of antioxidant defense systems, thereby leading to inhibition of tumor proliferation and metastasis [74]. Massive lipid peroxidation was observed only in A375 cell populations after 48 h ONC treatment, particularly in the A375R one (Figure 7). Consequently, in A375 cell populations, part of the cytotoxicity elicited by ONC could be ascribable to ferroptosis. Instead, ONC triggered early and sustained apoptotic cell death in all DAB-sensitive and DAB-resistant melanoma cells (Figures 6 and 7). Notably, this programmed cell death was more pronounced in melanoma cells resistant to BRAF inhibition and likely involves the mitochondrial pathway, as it was accompanied by increased levels of cleaved caspase-9 (Figure 6). The presence of a cell population undergoing apoptosis was further confirmed by flow cytometry, which revealed increased Annexin V/PI staining in all ONC-treated cells (Figure 7). In parallel, immunoblot analysis following cell preincubation with the pan-caspase inhibitor Z-VAD-FMK showed at least partial reduction in cleaved PARP expression levels (Figure 7). Previously, we demonstrated the inhibition by ONC of the antiapoptotic protein BCL2 in both BRAF-mutated and BRAF-wild-type melanoma cell lines [50], while, in the present study, survivin, another key antiapoptotic effector, was strongly downregulated in all melanoma cells 48 h after ONC treatment (Figure 6). Survivin is of particular interest because it is a known target of miR-34a. High expression of miR-34a, as previously reported after ONC treatment [51], can also suppress cell proliferation and migration and promote apoptosis in multiple cancer cell lines, including melanoma [75,76]. Consistently, Chen et al. reported that the delivery of miR-34a downregulates survivin and induces apoptosis in a mouse melanoma cell line [77].

Again, it is also well established that the transcription factor NRF2 is a target of miR-20a [78]. Thus, it can be hypothesized that the major effects of ONC on antioxidant defenses and apoptosis induction may be mediated by miRNAs. Notably, we recently showed that the circular RNA circ_0001591, which acts as a sponge for miR-20a and miR-34a, indirectly regulates the expression of the oncoproteins AXL and Fra1 [79]. Consistent with this mechanism, AXL and Fra1 were markedly downregulated by ONC treatment in A375P and FO-1P cells [51]. Whether ONC directly degrades this circular RNA and whether such an effect accounts for the observed increase in miR-20a and miR-34a levels are currently under investigation.

4. Materials and Methods

4.1. Expression and Purification of Recombinant ONC

The plasmid encoding for recombinant wt-ONC (pcDNA-ONC) was kindly provided by Prof. D. Picone and E. Pizzo (The University of Naples, Federico II). The ONC sequence was then inserted into a pET-22b (+) vector to express the enzyme in *E. coli*. Cells were centrifuged, and ONC was extracted and refolded from inclusion bodies, with a proper reduced and oxidized glutathione ratio, following the protocol described by Notomista and colleagues [44], slightly modified in [24]. The protein solution was concentrated with an Amicon 3 Plus ultrafilter (3 kDa cutoff, Merck-Millipore, Milan, Italy) and chromatographed with a Superdex 75 XK 26/60 preparative SEC column (Cytiva, Milan, Italy) attached to a ÄKTA Purifier system (Cytiva, Milan, Italy). Afterwards, the start Met(−1) was removed by incubating the SEC-purified ONC in a solution of a zinc-dependent aminopeptidase from *Aeromonas proteolytica* (AAP) dissolved in 0.200 M potassium phosphate, containing 25 μM $ZnSO_4$ and buffered at pH 8.0. The reaction was prolonged to 96 h, at 37 °C, at a

concentration of about 0.3 mg/mL, with an AAP:ONC molar ratio of about 1:1000, and was then blocked by adding 0.010 M EDTA, final concentration. The enzyme solution was concentrated again with another Amicon 3 Plus ultrafilter, and a final purification step was performed using the same Superdex 75 XK 26/60 preparative SEC column mentioned above attached to a ÄKTA-Purifier system. The elution profile was visualized and compared with the one obtained with 8 mg of "standard" RNase A (type XII A, R-5500, Sigma-Merck, Milan, Italy) by using the ÄKTA Unicorn 5.01 software.

4.2. Analysis of ONC Purity and Catalytic Activity

The SEC-purified ONC was first analyzed with mass spectrometry to assess if the Met(−1) removal was successful. To do so, a high-resolution Ultraflextreme MALDI-TOF/TOF spectrometer (Bruker Daltonics, Bremen, Deutscheland), of the "Centro Piattaforme Tecnologiche" (CPT) of the University of Verona, was used. The analysis was performed as described in [50], and data were analyzed using the instrument-associated Bruker Daltonics Flex Analysis Software, version 3.4.

The purified ONC was dialyzed against ddH_2O, concentrated with an Amicon 3 Plus ultrafilter, and lyophilized as 0.5 or 1.0 mg aliquots. Each ONC aliquot used for activity analysis was dissolved in 0.010 M sodium phosphate, pH 6.7, or in 1 × PBS, depending on the experiment to be performed.

ONC purity was assessed with a UV-Vis 240–500 nm scan using a Jasco V-750 spectrophotometer (Jasco Europe, Cremella (LC), Italy), and the concentration was measured at 280 nm, using for ONC an $\varepsilon^{1\%}_{280}$ = 0.87 [80], while $\varepsilon^{1\%}_{280}$ = 0.72 for RNase A [81].

The ONC enzymatic activity was measured at 25 °C, in parallel with RNase A, using a solution of about 0.5 mg/mL yeast ss-RNA as substrate, dissolved in 0.10 M sodium acetate/acetic acid buffer, pH 5.0, to obtain an initial Abs_{300} value comprised between 0.60 and 0.70. Yeast RNA is the gold standard substrate for RNase A, and ONC-RNase A compared assays were performed following the protocol described by Kunitz that exploits an absorbance tail decrease induced by the enzyme at 300 nm [43]. Abs_{300} variation was followed using the same Jasco V-750 spectropolarimeter, and the dAbs/dt slope of the initial, linear part of the curve was calculated with the instrument software. The ONC-specific activity (per mg) was calculated and compared with that of RNase A, as the average, ±S.D., of three different experiments.

4.3. Fluorescence Microscopic Analysis

4′,6-Diamidino-2-phenylindole dihydrochloride (DAPI) is a fluorescent dye that binds DNA through multiple binding modes and is retained in daughter cells during cell proliferation. Cells were seeded in 24-well plates at a density of 2.5 × 10^4 cells per well. After 24 h, cells were treated with 1 µM ONC for 48 h. Following treatment, the culture medium was removed by vacuum aspiration, and cells were fixed with 100 µL/well of 4% (*w*/*v*) paraformaldehyde (PFA) (AppliChem, Monza, Italy) for 10 min at room temperature (RT). The fixative was removed, and cells were washed three times with 1× Dulbecco's Phosphate-Buffered Saline (DPBS) (Gibco, BRL Invitrogen Corp., Carlsbad, CA, USA) for 10 min each on a shaker. Subsequently, cells were incubated with 100 µL/well of DAPI (1:1000 dilution; Thermo Fisher Scientific, Milan, Italy) for 15 min at RT. The staining solution was removed, and wells were washed three times, 10 min each, with 1× DPBS.

Fluorescence images were acquired using an Olympus Evident ApexView APX100 fluorescence microscope (Hamburg, Germany). Each experimental condition was performed in triplicate, and comparisons were made against the respective control samples.

4.4. Confocal Microscopy and Mitochondrial Network Analysis

Parental and DAB-resistant A375 and FO-1 cells were incubated with MitoTracker green FM (Ex490nm/Em516nm; Thermo Fisher Scientific, Milan, Italy) diluted 1:5000 in Opti-MEM for 30 min at 37 °C. Before image acquisition, the media was replaced with DMEM, no phenol red (Thermo Fisher Scientific, Milan, Italy). All images were acquired using an Evident FV4000 confocal microscope (Olympus, Milan, Italy) at 60× magnification (1.4 NA) oil immersion. After acquisition, all images were deconvolved using the Scientific Volume Imaging software (v18.10, Hilversum, The Netherlands) with the following parameters: deconvolution algorithm, classic maximum likelihood estimation (CMLE); maximum iterations, 100; SNR, 20; and quality threshold, 0.05. All images were then analyzed by the FiJi software (v1.54p, NIH, Bethesda, MD, USA) by using an existing plug-in.

4.5. Cell Viability Assay

Melanoma cells were seeded into 96-well plates at the following densities: A375, 2.9×10^3 cells/well; FO-1, 3.5×10^3 cells/well. After 24 h, cells were treated with 0.25, 0.5, 0.75, 1.0, or 1.5 μM ONC and incubated for 72 h. At the end of the treatment, cells were fixed by adding 25 μL/well of 50% (*w*/*v*) trichloroacetic acid directly to the culture medium. Plates were incubated at 4 °C for 1 h, washed four times with deionized water (ddH_2O), and air-dried at RT. Cells were then stained with 50 μL/well of 0.04% (*w*/*v*) sulforhodamine B (SRB) sodium salt solution (Sigma-Aldrich, Milan, Italy) and incubated for 1 h at RT. Excess dye was removed by rinsing with 1% acetic acid, and plates were air-dried. Bound SRB was solubilized in 10 mM Tris-base solution (pH 10.5), and absorbance was measured at 540 nm using a TECAN NanoQuant Infinite M200 Pro plate reader (Tecan Group Ltd., Männedorf, Switzerland). Each experimental condition was analyzed in five replicates.

4.6. Assessment of Intracellular ROS, Mitochondrial Superoxide, and Lipid Peroxidation Using Fluorescent Probes

Cells were seeded in triplicate in 48-well plates at a density of 1.5×10^4 cells/well. The following day, cells were treated with 1 μM ONC for 48 h. Intracellular oxidative stress was evaluated using three different fluorescent probes under the same experimental conditions. Total intracellular ROS levels were measured using the CellROX™ Deep Red probe (C10422, Invitrogen Corp., Carlsbad, CA, USA) according to the manufacturer's instructions. Mitochondrial superoxide production was assessed using MitoSOX™ Red Mitochondrial Superoxide Indicator for live-cell imaging (M36008, Invitrogen Corp., Carlsbad, CA, USA). Lipid peroxidation was evaluated using BODIPY™ 581/591 C11 (D3861, Invitrogen Corp., Carlsbad, CA, USA), a ratiometric fluorescent sensor of lipid oxidative damage.

After staining with the respective probes, cells were harvested, resuspended in flow buffer consisting of PBS supplemented with 2% FBS and 3 mM EDTA, and analyzed using a BD LSRFortessa flow cytometer (BD Biosciences, Milan, Italy). Flow cytometry data were analyzed using FlowJo software v10.8.1 (BD Biosciences, Milan, Italy). Fluorescence signals were quantified within the total cell population of each cell line. Data represent at least three independent biological replicates.

4.7. Assessment of Cell Death by Annexin V/Propidium Iodide Staining

Cells were seeded in triplicate in 48-well plates at a density of 1.5×10^4 cells/well. The following day, cells were treated with 1 μM ONC for 48 h. After treatment, both floating and adherent cells were collected, washed with cold PBS, and resuspended in Annexin V binding buffer according to the manufacturer's instructions. Cells were stained with Annexin V–FITC and propidium iodide (PI) using the Annexin V Apoptosis Detection Kit (88-8007-72, BD Biosciences, Milan, Italy) and incubated for 15 min at RT in the dark.

Following incubation, PI was added for 5 min, and samples were diluted with binding buffer for flow cytometry analysis using a BD LSRFortessa instrument (BD Biosciences, Milan, Italy). Annexin V–/PI–cells were considered viable. Flow cytometry data were analyzed using FlowJo software v10.8.1 (BD Biosciences, Milan, Italy). Data represent at least three independent biological replicates.

4.8. Labeling of Autophagic Vacuoles with Monodansylcadaverine (MDC)

Cells were seeded in five replicates into 96-well plates at the following densities: A375, 2.9×10^3 cells/well; FO-1, 3.5×10^3 cells/well. After 24 h, cells were either untreated or treated with 1.0 μM ONC for 48 h. To quantify autophagy induction, at the end of treatment, cells were incubated in culture medium containing the fluorescent probe MDC (50 μM; Sigma-Aldrich, Milan, Italy) at 37 °C for 15 min. Subsequently, cells were washed with Hanks' buffer (20 mM HEPES, pH 7.2; 10 mM glucose; 118 mM NaCl; 4.6 mM KCl; and 1 mM $CaCl_2$). Fluorescence was measured using a microplate reader (excitation 380 nm, emission 535 nm; NanoQuant Infinite M200 Pro, Tecan Group Ltd., Männedorf, Switzerland). The fluorescence values were normalized to cell mass determined by crystal violet assay. MDC incorporation was expressed as relative fluorescence intensity, with the fluorescence of untreated cells set to 1. Data represent at least three independent biological replicates.

4.9. Total Protein Extraction

Cells were seeded in 35 mm Petri dishes (A375: 8.0×10^4 cells/dish; FO-1: 9.0×10^4 cells/dish). After 24 h, cells were treated with 0.5 or 1 μM ONC or left untreated as controls. Following an additional 24 or 48 h treatment, cells were scraped in pre-warmed 1× sample buffer (2% SDS, 10% glycerol, 50 mM Tris-HCl, 1.75% β-mercaptoethanol, and bromophenol blue) and subsequently boiled at 98 °C for 10 min. In the experiments involving the caspase inhibitor, Z-VAD-FMK was added to the cell culture medium at a concentration of 25 μM. After 2 h of preincubation, 1 μM ONC was added, and cells were incubated for an additional 48 h. Total protein extracts were then stored at −80 °C until further analysis.

4.10. Immunoblot Analysis

Protein extracts were separated by SDS–PAGE using 8.5–14% polyacrylamide gels, and subsequently transferred onto polyvinylidene difluoride (PVDF) membranes (Merck Millipore, Milan, Italy), blocked for 1 h at RT in TBST buffer (10 mM Tris-HCl, pH 7.5; 100 mM NaCl; 0.1% Tween 20) containing 5% non-fat milk. Membranes were then incubated overnight at 4 °C with gentle agitation in 5% bovine serum albumin (BSA) containing the following primary antibodies: FTH1 (A19544); p(Ser40)-NRF2 (AP1133); HO-1 (A19062); GCLM (A11444); SLC7A11 (A2413); GSTP1 (A19061); FSP1 (A22278); cleaved PARP (A19612); LC3B (AA19665); p(T161)CDK1 (AP0324); p(Thr160)CDK2 (AP1364); p(Thr172)CDK4 (AP1364); p(ser616)-DRP1 (AP1353); FIS1 (A19666); PINK1 (A24745); ATPB (A11214); pERK1/2 (AP0974); ERK1/2 (A16686); UQCRC1 (A26343); (Abclonal, Woburn, MA, USA); ATG3 (GTX128065); Beclin1 (GTX133555); SOD2 (GTX630559); Glutathione reductase (GTX114199); COX4 (GTX114330); c-Myc (GTX103436); (GeneTex, Irvine, CA, USA); Mitofusin-1 (#14739); Mitofusin-2 (#11925); DRP1 (#8570); OPA1 (#80471); TOM20 (#42406); GAPDH (#2118); p(Tyr605)-STAT3 (#9145); p(Ser536)P65-NF-kB (#3033); cleaved Caspase 9 (#9509) (Cell Signaling Technology, Danvers, MA, USA); PGC1α (PA5-38022) (Invitrogen, Life Technologies, Monza, Italy); γ-H2AX (29380-1); Survivin (66495-1-Ig); and β-actin (66031-1) (Proteintech, Manchester, UK). After primary antibody incubation, membranes were washed three times for 10 min each with TBST and then incubated for 1 h at RT with horseradish peroxidase (HRP)-conjugated anti-rabbit or anti-mouse secondary

antibodies (Cell Signaling Technology, Danvers, MA, USA). Membranes were subsequently washed three additional times for 10 min each with TBST. Protein expression levels were normalized to β-actin. Immunoreactive bands were detected using an enhanced chemiluminescence (ECL) kit (Merck Millipore, Milan, Italy) and visualized with a ChemiDoc imaging system (Bio-Rad, Hercules, CA, USA).

4.11. Statistics

The results are presented as the mean value ± standard deviation (S.D.). Statistical differences were analyzed using the GraphPad Prism, statistical program, version 8.0.2, employing an unpaired ANOVA test, unless otherwise stated. A *p*-value less than 0.05 (*), or less than 0.01 (**) was considered to be statistically significant. Each type of experiment was conducted with a minimum of three independent biological replicates. The normal distribution of the data was assessed using the Shapiro–Wilk test.

5. Conclusions

The amphibian ribonuclease ONC demonstrates here the ability to counteract the malignant phenotype of two BRAF-mutated melanoma cell lines, including both DAB-sensitive and -resistant subpopulations. ONC treatment induced elevated levels of reactive oxygen species and reduced the expression of multiple antioxidant-related proteins, most notably NRF2. Furthermore, ONC impaired mitochondrial biogenesis and fission without inducing mitophagy, hence suggesting a lowered mitochondrial functionality. ONC also triggered sustained apoptosis via the mitochondrial pathway and markedly inhibited survivin expression. Notably, these anti-melanoma effects were more pronounced in DAB-resistant melanoma cells.

ONC influences multiple molecular targets and modulates noncoding RNA biogenesis and processing [82], suggesting that its biological effects stem from the convergence of multiple regulatory pathways.

Although the precise molecular mechanisms underlying its activity are not yet fully understood, this study advances current knowledge and further confirms the anti-melanoma properties of ONC, particularly in BRAF inhibitor–resistant melanoma cell lines.

Supplementary Materials: The following supporting information can be downloaded at: https://www.mdpi.com/article/10.3390/ijms27041638/s1.

Author Contributions: Conceptualization, M.M. and G.G.; methodology, A.F. and A.C. (Alessia Cardile); investigation, C.P., A.C. (Alessia Cardile), A.F., F.Z., V.Z., F.D., A.C. (Adriana Celesia) and R.P.; resources, A.F., G.G. and M.M.; writing—original draft preparation, G.G. and M.M.; writing—review and editing, G.G. and M.M.; supervision, M.M.; funding acquisition, A.F., G.G. and M.M. All authors have read and agreed to the published version of the manuscript.

Funding: This work was supported by the Associazione Italiana per la Ricerca sul Cancro (Individual Grant—MFAG, AIRC, Project: 27080, P.I. Alessandra Fiore).

Institutional Review Board Statement: Not applicable.

Informed Consent Statement: Not applicable.

Data Availability Statement: The original contributions presented in this study are included in the article/Supplementary Material. Further inquiries can be directed to the corresponding authors.

Acknowledgments: We acknowledge the "Centro Piattaforme Tecnologiche" (CPT) of the University of Verona for providing mass spectrometry facilities and technical assistance, and Daniela Sorio (CPT) for the relative measurements and analyses.

Conflicts of Interest: The authors declare no conflicts of interest.

References

1. Giannitti, G.; Paganoni, A.J.J.; Marchesi, S.; Garavaglia, R.; Fontana, F. Mitochondrial Bioenergetics and Networks in Melanoma: An Update. *Apoptosis Int. J. Program. Cell Death* **2025**, *30*, 2042–2056. [CrossRef]
2. Boutros, A.; Croce, E.; Ferrari, M.; Gili, R.; Massaro, G.; Marconcini, R.; Arecco, L.; Tanda, E.T.; Spagnolo, F. The Treatment of Advanced Melanoma: Current Approaches and New Challenges. *Crit. Rev. Oncol. Hematol.* **2024**, *196*, 104276. [CrossRef] [PubMed]
3. Flaherty, K.T.; Puzanov, I.; Kim, K.B.; Ribas, A.; McArthur, G.A.; Sosman, J.A.; O'Dwyer, P.J.; Lee, R.J.; Grippo, J.F.; Nolop, K.; et al. Inhibition of Mutated, Activated BRAF in Metastatic Melanoma. *N. Engl. J. Med.* **2010**, *363*, 809–819. [CrossRef]
4. Wan, P.T.C.; Garnett, M.J.; Roe, S.M.; Lee, S.; Niculescu-Duvaz, D.; Good, V.M.; Jones, C.M.; Marshall, C.J.; Springer, C.J.; Barford, D.; et al. Mechanism of Activation of the RAF-ERK Signaling Pathway by Oncogenic Mutations of B-RAF. *Cell* **2004**, *116*, 855–867. [CrossRef]
5. Bollag, G.; Hirth, P.; Tsai, J.; Zhang, J.; Ibrahim, P.N.; Cho, H.; Spevak, W.; Zhang, C.; Zhang, Y.; Habets, G.; et al. Clinical Efficacy of a RAF Inhibitor Needs Broad Target Blockade in BRAF-Mutant Melanoma. *Nature* **2010**, *467*, 596–599. [CrossRef] [PubMed]
6. Loftus, A.W.; Zarei, M.; Kakish, H.; Hajihassani, O.; Hue, J.J.; Boutros, C.; Graor, H.J.; Nakazzi, F.; Bahlibi, T.; Winter, J.M.; et al. Therapeutic Implications of the Metabolic Changes Associated with BRAF Inhibition in Melanoma. *Cancer Treat. Rev.* **2024**, *129*, 102795. [CrossRef]
7. Hauschild, A.; Grob, J.-J.; Demidov, L.V.; Jouary, T.; Gutzmer, R.; Millward, M.; Rutkowski, P.; Blank, C.U.; Miller, W.H.; Kaempgen, E.; et al. Dabrafenib in BRAF-Mutated Metastatic Melanoma: A Multicentre, Open-Label, Phase 3 Randomised Controlled Trial. *Lancet* **2012**, *380*, 358–365. [CrossRef]
8. Luebker, S.A.; Koepsell, S.A. Diverse Mechanisms of BRAF Inhibitor Resistance in Melanoma Identified in Clinical and Preclinical Studies. *Front. Oncol.* **2019**, *9*, 268. [CrossRef]
9. Ratnikov, B.I.; Scott, D.A.; Osterman, A.L.; Smith, J.W.; Ronai, Z.A. Metabolic Rewiring in Melanoma. *Oncogene* **2017**, *36*, 147–157. [CrossRef]
10. Puigserver, P.; Spiegelman, B.M. Peroxisome Proliferator-Activated Receptor-Gamma Coactivator 1 Alpha (PGC-1 Alpha): Transcriptional Coactivator and Metabolic Regulator. *Endocr. Rev.* **2003**, *24*, 78–90. [CrossRef] [PubMed]
11. Fontana, F.; Macchi, C.; Anselmi, M.; Rizzuto, A.S.; Ruscica, M.; Limonta, P. PGC1-α-Driven Mitochondrial Biogenesis Contributes to a Cancer Stem Cell Phenotype in Melanoma. *Biochim. Biophys. Acta Mol. Basis Dis.* **2024**, *1870*, 166897. [CrossRef]
12. Giacomello, M.; Pyakurel, A.; Glytsou, C.; Scorrano, L. The Cell Biology of Mitochondrial Membrane Dynamics. *Nat. Rev. Mol. Cell Biol.* **2020**, *21*, 204–224. [CrossRef] [PubMed]
13. Adebayo, M.; Singh, S.; Singh, A.P.; Dasgupta, S. Mitochondrial Fusion and Fission: The Fine-Tune Balance for Cellular Homeostasis. *FASEB J. Off. Publ. Fed. Am. Soc. Exp. Biol.* **2021**, *35*, e21620. [CrossRef] [PubMed]
14. Zhao, Z.; Ren, Y.; Yuan, M.; Liu, G.; Sun, J. The Molecular Mechanisms of Mitochondrial Dynamics and Mitophagy and Their Complex Association with Cancer Drug Resistance. *J. Transl. Med.* **2025**, *23*, 1047. [CrossRef]
15. Song, Y.; Ren, S.; Chen, X.; Li, X.; Chen, L.; Zhao, S.; Zhang, Y.; Shen, X.; Chen, Y. Inhibition of MFN1 Restores Tamoxifen-Induced Apoptosis in Resistant Cells by Disrupting Aberrant Mitochondrial Fusion Dynamics. *Cancer Lett.* **2024**, *590*, 216847. [CrossRef] [PubMed]
16. Sharma, A.; Virmani, T.; Kumar, G.; Sharma, A.; Virmani, R.; Gugulothu, D.; Singh, K.; Misra, S.K.; Pathak, K.; Chitranshi, N.; et al. Mitochondrial Signaling Pathways and Their Role in Cancer Drug Resistance. *Cell. Signal.* **2024**, *122*, 111329. [CrossRef]
17. Yamashita, K.; Miyata, H.; Makino, T.; Masuike, Y.; Furukawa, H.; Tanaka, K.; Miyazaki, Y.; Takahashi, T.; Kurokawa, Y.; Yamasaki, M.; et al. High Expression of the Mitophagy-Related Protein Pink1 Is Associated with a Poor Response to Chemotherapy and a Poor Prognosis for Patients Treated with Neoadjuvant Chemotherapy for Esophageal Squamous Cell Carcinoma. *Ann. Surg. Oncol.* **2017**, *24*, 4025–4032. [CrossRef]
18. Chan, N.C.; Salazar, A.M.; Pham, A.H.; Sweredoski, M.J.; Kolawa, N.J.; Graham, R.L.J.; Hess, S.; Chan, D.C. Broad Activation of the Ubiquitin–Proteasome System by Parkin Is Critical for Mitophagy. *Hum. Mol. Genet.* **2011**, *20*, 1726–1737. [CrossRef]
19. Eller, S.; Ebner, S.; Haselrieder, C.; Günther, J.K.; Drasche, A.; Strich, S.; Volani, C.; Medici, A.; Nikolajevic, A.; Deltedesco, A.; et al. Exploiting Metabolic Adaptations to Overcome Dabrafenib Treatment Resistance in Melanoma Cells. *Mol. Oncol.* **2025**. *Online ahead of print*. [CrossRef]
20. Zanrè, V.; Bellinato, F.; Cardile, A.; Passarini, C.; Di Bella, S.; Menegazzi, M. BRAF-Mutated Melanoma Cell Lines Develop Distinct Molecular Signatures After Prolonged Exposure to AZ628 or Dabrafenib: Potential Benefits of the Antiretroviral Treatments Cabotegravir or Doravirine on BRAF-Inhibitor-Resistant Cells. *Int. J. Mol. Sci.* **2024**, *25*, 11939. [CrossRef]
21. Ardelt, W.; Mikulski, S.M.; Shogen, K. Amino Acid Sequence of an Anti-Tumor Protein from Rana Pipiens Oocytes and Early Embryos. Homology to Pancreatic Ribonucleases. *J. Biol. Chem.* **1991**, *266*, 245–251. [CrossRef] [PubMed]
22. Raines, R.T. Ribonuclease A. *Chem. Rev.* **1998**, *98*, 1045–1066. [CrossRef]
23. Mosimann, S.C.; Ardelt, W.; James, M.N. Refined 1.7 A X-Ray Crystallographic Structure of P-30 Protein, an Amphibian Ribonuclease with Anti-Tumor Activity. *J. Mol. Biol.* **1994**, *236*, 1141–1153. [CrossRef]

24. Fagagnini, A.; Pica, A.; Fasoli, S.; Montioli, R.; Donadelli, M.; Cordani, M.; Butturini, E.; Acquasaliente, L.; Picone, D.; Gotte, G. Onconase Dimerization through 3D Domain Swapping: Structural Investigations and Increase in the Apoptotic Effect in Cancer Cells. *Biochem. J.* **2017**, *474*, 3767–3781. [CrossRef]
25. Suhasini, A.N.; Sirdeshmukh, R. Transfer RNA Cleavages by Onconase Reveal Unusual Cleavage Sites. *J. Biol. Chem.* **2006**, *281*, 12201–12209. [CrossRef]
26. Qiao, M.; Zu, L.-D.; He, X.-H.; Shen, R.-L.; Wang, Q.-C.; Liu, M.-F. Onconase Downregulates MicroRNA Expression through Targeting MicroRNA Precursors. *Cell Res.* **2012**, *22*, 1199–1202. [CrossRef]
27. Saxena, A.; Saxena, S.K.; Shogen, K. Effect of Onconase on Double-Stranded RNA in Vitro. *Anticancer Res.* **2009**, *29*, 1067–1071. [PubMed]
28. Saxena, S.K.; Gravell, M.; Wu, Y.N.; Mikulski, S.M.; Shogen, K.; Ardelt, W.; Youle, R.J. Inhibition of HIV-1 Production and Selective Degradation of Viral RNA by an Amphibian Ribonuclease. *J. Biol. Chem.* **1996**, *271*, 20783–20788. [CrossRef] [PubMed]
29. Hodge, T.; Draper, K.; Brasel, T.; Freiberg, A.; Squiquera, L.; Sidransky, D.; Sulley, J.; Taxman, D.J. Antiviral Effect of Ranpirnase Against Ebola Virus. *Antivir. Res.* **2016**, *132*, 210–218. [CrossRef]
30. Darzynkiewicz, Z.; Carter, S.P.; Mikulski, S.M.; Ardelt, W.J.; Shogen, K. Cytostatic and Cytotoxic Effects of Pannon (P-30 Protein), a Novel Anticancer Agent. *Cell Tissue Kinet.* **1988**, *21*, 169–182. [CrossRef]
31. Wang, X.-M.; Guo, Z.-Y. Recombinant Expression, Different Downstream Processing of the Disulfide-Rich Anti-Tumor Peptide Ranpirnase and Its Effect on the Growth of Human Glioma Cell Line SHG-44. *Biomed. Rep.* **2013**, *1*, 747–750. [CrossRef]
32. Smolewski, P.; Witkowska, M.; Zwolinska, M.; Cebula-Obrzut, B.; Majchrzak, A.; Jeske, A.; Darzynkiewicz, Z.; Ardelt, W.; Ardelt, B.; Robak, T. Cytotoxic Activity of the Amphibian Ribonucleases Onconase and R-Amphinase on Tumor Cells from B Cell Lymphoproliferative Disorders. *Int. J. Oncol.* **2014**, *45*, 419–425. [CrossRef]
33. Fiorini, C.; Cordani, M.; Gotte, G.; Picone, D.; Donadelli, M. Onconase Induces Autophagy Sensitizing Pancreatic Cancer Cells to Gemcitabine and Activates Akt/MTOR Pathway in a ROS-Dependent Manner. *Biochim. Biophys. Acta* **2015**, *1853*, 549–560. [CrossRef] [PubMed]
34. Raineri, A.; Prodomini, S.; Fasoli, S.; Gotte, G.; Menegazzi, M. Influence of Onconase in the Therapeutic Potential of PARP Inhibitors in A375 Malignant Melanoma Cells. *Biochem. Pharmacol.* **2019**, *167*, 173–181. [CrossRef]
35. Mikulski, S.; Chun, H.; Mittelman, A.; Panella, T.; Puccio, C.; Shogen, K.; Costanzi, J. Relationship Between Response Rate and Median Survival in Patients with Advanced Nonsmall Cell Lung-Cancer—Comparison of Onconase(r) with Other Anticancer Agents. *Int. J. Oncol.* **1995**, *6*, 889–897. [CrossRef]
36. Pavlakis, N.; Vogelzang, N.J. Ranpirnase—An Antitumour Ribonuclease: Its Potential Role in Malignant Mesothelioma. *Expert Opin. Biol. Ther.* **2006**, *6*, 391–399. [CrossRef] [PubMed]
37. Kobe, B.; Deisenhofer, J. Mechanism of Ribonuclease Inhibition by Ribonuclease Inhibitor Protein Based on the Crystal Structure of Its Complex with Ribonuclease. *A. J. Mol. Biol.* **1996**, *264*, 1028–1043. [CrossRef]
38. Rutkoski, T.J.; Raines, R.T. Evasion of Ribonuclease Inhibitor as a Determinant of Ribonuclease Cytotoxicity. *Curr. Pharm. Biotechnol.* **2008**, *9*, 185–189. [CrossRef] [PubMed]
39. Turcotte, R.F.; Lavis, L.D.; Raines, R.T. Onconase Cytotoxicity Relies on the Distribution of Its Positive Charge. *FEBS J.* **2009**, *276*, 3846–3857. [CrossRef]
40. Sundlass, N.K.; Eller, C.H.; Cui, Q.; Raines, R.T. Contribution of Electrostatics to the Binding of Pancreatic-Type Ribonucleases to Membranes. *Biochemistry* **2013**, *52*, 6304–6312. [CrossRef]
41. Ardelt, W.; Shogen, K.; Darzynkiewicz, Z. Onconase and Amphinase, the Antitumor Ribonucleases from Rana Pipiens Oocytes. *Curr. Pharm. Biotechnol.* **2008**, *9*, 215–225. [CrossRef]
42. Lee, J.E.; Raines, R.T. Contribution of Active-Site Residues to the Function of Onconase, a Ribonuclease with Antitumoral Activity. *Biochemistry* **2003**, *42*, 11443–11450. [CrossRef]
43. Kunitz, M. A Spectrophotometric Method for the Measurement of Ribonuclease Activity. *J. Biol. Chem.* **1946**, *164*, 563–568. [CrossRef]
44. Notomista, E.; Cafaro, V.; Fusiello, R.; Bracale, A.; D'Alessio, G.; Di Donato, A. Effective Expression and Purification of Recombinant Onconase, an Antitumor Protein. *FEBS Lett.* **1999**, *463*, 211–215. [CrossRef] [PubMed]
45. An, Y.; Zhang, Q.; Zhao, J.; Zheng, N. Tangeretin Regulates Oxidative Stress in Cutaneous Melanoma Cells via the Nrf2 Signaling Pathway. *Arch. Dermatol. Res.* **2025**, *317*, 550. [CrossRef] [PubMed]
46. Löbrich, M.; Shibata, A.; Beucher, A.; Fisher, A.; Ensminger, M.; Goodarzi, A.A.; Barton, O.; Jeggo, P.A. ΓH2AX Foci Analysis for Monitoring DNA Double-Strand Break Repair: Strengths, Limitations and Optimization. *Cell Cycle* **2010**, *9*, 662–669. [CrossRef] [PubMed]
47. Doll, S.; Freitas, F.P.; Shah, R.; Aldrovandi, M.; da Silva, M.C.; Ingold, I.; Goya Grocin, A.; Xavier da Silva, T.N.; Panzilius, E.; Scheel, C.H.; et al. FSP1 Is a Glutathione-Independent Ferroptosis Suppressor. *Nature* **2019**, *575*, 693–698. [CrossRef]

48. Graves, J.A.; Wang, Y.; Sims-Lucas, S.; Cherok, E.; Rothermund, K.; Branca, M.F.; Elster, J.; Beer-Stolz, D.; Van Houten, B.; Vockley, J.; et al. Mitochondrial Structure, Function and Dynamics Are Temporally Controlled by c-Myc. *PLoS ONE* **2012**, *7*, e37699. [CrossRef]
49. Li, L.; Meng, Y.; Wu, X.; Li, J.; Sun, Y. Bromodomain-Containing Protein 4 Inhibitor JQ1 Promotes Melanoma Cell Apoptosis by Regulating Mitochondrial Dynamics. *Cancer Sci.* **2021**, *112*, 4013–4025. [CrossRef]
50. Gotte, G.; Campagnari, R.; Loreto, D.; Bettin, I.; Calzetti, F.; Menegazzi, M.; Merlino, A. The Crystal Structure of the Domain-Swapped Dimer of Onconase Highlights Some Catalytic and Antitumor Activity Features of the Enzyme. *Int. J. Biol. Macromol.* **2021**, *191*, 560–571. [CrossRef]
51. De Tomi, E.; Campagnari, R.; Orlandi, E.; Cardile, A.; Zanrè, V.; Menegazzi, M.; Gomez-Lira, M.; Gotte, G. Upregulation of MiR-34a-5p, MiR-20a-3p and MiR-29a-3p by Onconase in A375 Melanoma Cells Correlates with the Downregulation of Specific Onco-Proteins. *Int. J. Mol. Sci.* **2022**, *23*, 1647. [CrossRef]
52. Silva, C.M. Role of STATs as Downstream Signal Transducers in Src Family Kinase-Mediated Tumorigenesis. *Oncogene* **2004**, *23*, 8017–8023. [CrossRef] [PubMed]
53. Mohassab, A.M.; Hassan, H.A.; Abdelhamid, D.; Abdel-Aziz, M. STAT3 Transcription Factor as Target for Anti-Cancer Therapy. *Pharmacol. Rep. PR* **2020**, *72*, 1101–1124. [CrossRef] [PubMed]
54. Madonna, G.; Ullman, C.D.; Gentilcore, G.; Palmieri, G.; Ascierto, P.A. NF-KB as Potential Target in the Treatment of Melanoma. *J. Transl. Med.* **2012**, *10*, 53. [CrossRef] [PubMed]
55. Trotta, A.P.; Gelles, J.D.; Serasinghe, M.N.; Loi, P.; Arbiser, J.L.; Chipuk, J.E. Disruption of Mitochondrial Electron Transport Chain Function Potentiates the Pro-Apoptotic Effects of MAPK Inhibition. *J. Biol. Chem.* **2017**, *292*, 11727–11739. [CrossRef]
56. Altieri, D.C. Survivin, Versatile Modulation of Cell Division and Apoptosis in Cancer. *Oncogene* **2003**, *22*, 8581–8589. [CrossRef]
57. McKenzie, J.A.; Grossman, D. Role of the Apoptotic and Mitotic Regulator Survivin in Melanoma. *Anticancer Res.* **2012**, *32*, 397–404.
58. Gumeni, S.; Papanagnou, E.-D.; Manola, M.S.; Trougakos, I.P. Nrf2 Activation Induces Mitophagy and Reverses Parkin/Pink1 Knock down-Mediated Neuronal and Muscle Degeneration Phenotypes. *Cell Death Dis.* **2021**, *12*, 671. [CrossRef] [PubMed]
59. Song, S.; Tan, J.; Miao, Y.; Li, M.; Zhang, Q. Crosstalk of Autophagy and Apoptosis: Involvement of the Dual Role of Autophagy under ER Stress. *J. Cell. Physiol.* **2017**, *232*, 2977–2984. [CrossRef]
60. Niezgoda, A.; Niezgoda, P.; Czajkowski, R. Novel Approaches to Treatment of Advanced Melanoma: A Review on Targeted Therapy and Immunotherapy. *BioMed Res. Int.* **2015**, *2015*, 851387. [CrossRef]
61. Kakadia, S.; Yarlagadda, N.; Awad, R.; Kundranda, M.; Niu, J.; Naraev, B.; Mina, L.; Dragovich, T.; Gimbel, M.; Mahmoud, F. Mechanisms of Resistance to BRAF and MEK Inhibitors and Clinical Update of US Food and Drug Administration-Approved Targeted Therapy in Advanced Melanoma. *OncoTargets Ther.* **2018**, *11*, 7095–7107. [CrossRef]
62. Raineri, A.; Fasoli, S.; Campagnari, R.; Gotte, G.; Menegazzi, M. Onconase Restores Cytotoxicity in Dabrafenib-Resistant A375 Human Melanoma Cells and Affects Cell Migration, Invasion and Colony Formation Capability. *Int. J. Mol. Sci.* **2019**, *20*, 5980. [CrossRef]
63. Arslanbaeva, L.R.; Santoro, M.M. Adaptive Redox Homeostasis in Cutaneous Melanoma. *Redox Biol.* **2020**, *37*, 101753. [CrossRef] [PubMed]
64. Panieri, E.; Santoro, M.M. ROS Homeostasis and Metabolism: A Dangerous Liason in Cancer Cells. *Cell Death Dis.* **2016**, *7*, e2253. [CrossRef]
65. Hintsala, H.-R.; Jokinen, E.; Haapasaari, K.-M.; Moza, M.; Ristimäki, A.; Soini, Y.; Koivunen, J.; Karihtala, P. Nrf2/Keap1 Pathway and Expression of Oxidative Stress Lesions 8-Hydroxy-2′-Deoxyguanosine and Nitrotyrosine in Melanoma. *Anticancer Res.* **2016**, *36*, 1497–1506.
66. Chiang, S.-K.; Chen, S.-E.; Chang, L.-C. A Dual Role of Heme Oxygenase-1 in Cancer Cells. *Int. J. Mol. Sci.* **2018**, *20*, 39. [CrossRef]
67. Carpenter, E.L.; Becker, A.L.; Indra, A.K. NRF2 and Key Transcriptional Targets in Melanoma Redox Manipulation. *Cancers* **2022**, *14*, 1531. [CrossRef] [PubMed]
68. Yuan, L.; Mishra, R.; Patel, H.; Alanazi, S.; Wei, X.; Ma, Z.; Garrett, J.T. BRAF Mutant Melanoma Adjusts to BRAF/MEK Inhibitors via Dependence on Increased Antioxidant SOD2 and Increased Reactive Oxygen Species Levels. *Cancers* **2020**, *12*, 1661. [CrossRef] [PubMed]
69. Barrera, G.; Cucci, M.A.; Grattarola, M.; Dianzani, C.; Muzio, G.; Pizzimenti, S. Control of Oxidative Stress in Cancer Chemoresistance: Spotlight on Nrf2 Role. *Antioxid. Basel Switz.* **2021**, *10*, 510. [CrossRef]
70. Vazquez, F.; Lim, J.-H.; Chim, H.; Bhalla, K.; Girnun, G.; Pierce, K.; Clish, C.B.; Granter, S.R.; Widlund, H.R.; Spiegelman, B.M.; et al. PGC1α Expression Defines a Subset of Human Melanoma Tumors with Increased Mitochondrial Capacity and Resistance to Oxidative Stress. *Cancer Cell* **2013**, *23*, 287–301. [CrossRef]
71. Rossi, T.; Torcasio, R.; Ganino, L.; Valentino, I.; Boni, C.; Gentile, M.; Neri, A.; Amodio, N.; Pistoni, M. Dysregulated Mitochondrial Dynamics in Cancer: Unlocking New Strategies to Combat Drug Resistance. *Biochim. Biophys. Acta Rev. Cancer* **2025**, *1881*, 189510. [CrossRef]

72. Agir, N.; Georgakopoulos-Soares, I.; Zaravinos, A. A Multi-Omics Analysis of a Mitophagy-Related Signature in Pan-Cancer. *Int. J. Mol. Sci.* **2025**, *26*, 448. [CrossRef]
73. Ferraz, L.S.; da Costa, R.T.; da Costa, C.A.; Ribeiro, C.A.J.; Arruda, D.C.; Maria-Engler, S.S.; Rodrigues, T. Targeting Mitochondria in Melanoma: Interplay between MAPK Signaling Pathway and Mitochondrial Dynamics. *Biochem. Pharmacol.* **2020**, *178*, 114104. [CrossRef] [PubMed]
74. Tao, R.; Li, Y.; Gong, S.; Zhang, Q.; Zhu, Z. Unveiling Intricating Roles and Mechanisms of Ferroptosis in Melanoma. *Biochim. Biophys. Acta Rev. Cancer* **2025**, *1880*, 189234. [CrossRef]
75. Yan, D.; Zhou, X.; Chen, X.; Hu, D.-N.; Dong, X.D.; Wang, J.; Lu, F.; Tu, L.; Qu, J. MicroRNA-34a Inhibits Uveal Melanoma Cell Proliferation and Migration Through Downregulation of c-Met. *Invest. Ophthalmol. Vis. Sci.* **2009**, *50*, 1559–1565. [CrossRef]
76. Li, Y.; Guessous, F.; Zhang, Y.; Dipierro, C.; Kefas, B.; Johnson, E.; Marcinkiewicz, L.; Jiang, J.; Yang, Y.; Schmittgen, T.D.; et al. MicroRNA-34a Inhibits Glioblastoma Growth by Targeting Multiple Oncogenes. *Cancer Res.* **2009**, *69*, 7569–7576. [CrossRef] [PubMed]
77. Chen, Y.; Zhu, X.; Zhang, X.; Liu, B.; Huang, L. Nanoparticles Modified With Tumor-Targeting ScFv Deliver SiRNA and MiRNA for Cancer Therapy. *Mol. Ther.* **2010**, *18*, 1650–1656. [CrossRef]
78. Li, S.; Jin, S.; Chen, W.; Yu, J.; Fang, P.; Zhou, G.; Li, J.; Jin, L.; Chen, Y.; Chen, P.; et al. Mangiferin Alleviates Endoplasmic Reticulum Stress in Acute Liver Injury by Regulating the MiR-20a/MiR-101a-Nrf2 Axis. *J. Biochem.* **2020**, *168*, 365–374. [CrossRef]
79. Orlandi, E.; De Tomi, E.; Belpinati, F.; Menegazzi, M.; Gomez-Lira, M.; Romanelli, M.G.; Trabetti, E. Circular RNA Circ_0001591 Contributes to Melanoma Cell Migration Through AXL and FRA1 Proteins by Targeting MiR-20a-3p and MiR-34a-5p. *Genes* **2025**, *16*, 921. [CrossRef]
80. Leland, P.A.; Schultz, L.W.; Kim, B.M.; Raines, R.T. Ribonuclease A Variants with Potent Cytotoxic Activity. *Proc. Natl. Acad. Sci. USA* **1998**, *95*, 10407–10412. [CrossRef] [PubMed]
81. Wang, D.; Moore, S. Polyspermine-Ribonuclease Prepared by Cross-Linkage with Dimethyl Suberimidate. *Biochemistry* **1977**, *16*, 2937–2942. [CrossRef] [PubMed]
82. Menegazzi, M.; Gotte, G. Role of the Ribonuclease ONCONASE in MiRNA Biogenesis and TRNA Processing: Focus on Cancer and Viral Infections. *Int. J. Mol. Sci.* **2022**, *23*, 6556. [CrossRef] [PubMed]